J. metamorphic Geol., 2003, **21,** 377–393

The metamorphic field gradient in the eclogite type locality, Koralpe region, Eastern Alps

V. TENCZER AND K. STÜWE
Department of Geology and Paleontology, University of Graz, Heinrichstrasse 26, A-8010 Graz, Austria
(veronika.tenczer@uni-graz.at)

ABSTRACT The eclogite type locality in the Eastern Alps (the Koralpe and Saualpe region) is the largest region in the Eastern Alps that preserves high-pressure metamorphic rocks from the Eo-Alpine orogenic event of the Cretaceous age. Thermobarometric data from the metapelitic gneisses in the region indicate that a metamorphic field gradient across the region can be divided into three parts. The northern part shows continuously increasing P–T from 10 ± 1.5 to 14 ± 1.5 kbar and 500 ± 68 to 700 ± 68 °C over a distance of 40 km. The continuous increase in P–T indicates that no major tectonic boundaries were active in this part during the Eo-Alpine orogeny. Small discontinuities in the pressure gradient of the northern part can be correlated with more localized deformation. The central part exposes amphibolite–eclogite facies rocks with 15 ± 1.5 kbar and 700 ± 68 °C over about 20 km length. The southern part shows decreasing P–T conditions from 15 ± 1.5 to 10 ± 1.5 kbar and 700 ± 68 to 600 ± 63 °C over a distance of 10 km beyond which conditions remain roughly constant for the remainder of the profile.

Overall, the field gradient is characterized by: (i) an *increase* in age with *decreasing* metamorphic grade and (ii) a T/P ratio that is *lower* than common metamorphic geotherms. The age–grade relationship is *consistent* with the timing relationship along piezothermal arrays predicted by simple models for regional metamorphism. However, the T/P ratio of the field gradient is *inconsistent* with such an interpretation. These inconsistencies indicate that the profile is not simply an obliquely exposed crustal section. We suggest that the exhumation of the transect is best explained with a two dimensional model of an extruding wedge, as has recently been suggested as a typical scenario for other large scale compressional orogens.

Keywords: eclogite type locality; Koralpe; metamorphic field gradient.

INTRODUCTION

The formation of the Eastern Alps was driven by two major orogenic events that occurred in the Cretaceous and Oligocene. The Cretaceous event is generally called the 'Eo-Alpine' event (Thöni & Jagoutz, 1992; Thöni & Miller, 1996; Miller & Thöni, 1997) and is the focus of this paper. The Oligocene event is known as the 'Tauern' event (Inger & Cliff, 1994) and is mainly recorded by rocks exposed in the Tauern Window, where the metamorphic conditions and gradients have been studied in detail (Kurz *et al.*, 1996, 1998; Lammerer & Weger, 1998). The Tauern event correlates with the Oligocene event observed in much of the central and western Alps (Droop *et al.*, 1990) where metamorphic field gradients have been studied, as in the Lepontine, for example (Todd & Engi, 1997). The Cretaceous event is recorded by all cover nappes around the Tauern window and constitutes the most wide spread metamorphic event in the eastern Alps. However, there are only two large regions where rocks of amphibolite and eclogite facies (Eo-Alpine metamorphic grade) are exposed. These two areas are conspicuously oriented symmetrically around the Tauern Window (Frey *et al.*, 1999). They include: (i) the southern Ötztal region (including the Schneeberg complex) in the west and (ii) substantial parts of the Koralpe–Saualpe region in the east (Fig. 1). The Koralpe–Saualpe region is by far the largest region and also contains the type locality for eclogite (Hauy, 1822). In both the Ötztal and the Koralpe–Saualpe regions, a north–south metamorphic field gradient is exposed that ranges from greenschist to eclogite facies metamorphic conditions (Konzett & Hoinkes, 1991, 1996; Hoinkes *et al.*, 1987, 1991). This metamorphic field gradient encompasses both pelitic sequences and mafic intercalations which occur as eclogitized lenses in the high grade parts of both the Ötztal and the Koralpe–Saualpe transects (Miller & Thöni, 1997; Thöni & Jagoutz, 1992, 1993). The highest grade parts of both the Ötztal and the Koralpe–Saualpe transects have been studied in the past (Ehlers *et al.*, 1994; Stüwe & Powell, 1995) and heat transfer mechanisms potentially responsible for the Eo-Alpine metamorphic event have been discussed by Stüwe (1998). However, many of the interpretations of heat transfer mechanisms in the Koralpe remain ill-constrained as no detailed description of the metamorphic field gradient exists.

In this paper we present the first detailed documentation of the metamorphic field gradient in

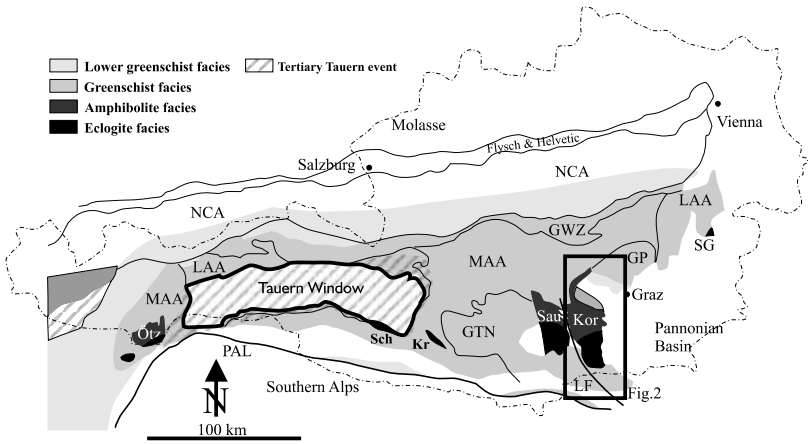

Fig. 1. Regional distribution and degree of Eoalpine metamorphism in the Eastern Alps (modified after Frey *et al*., 1999). NCA = Northern Calcareous Alps, PAL = Periadriatic Lineament, GWZ = Greywacke Zone, MAA = Middle Austroalpine, LAA = lower Austroalpine, GP = Palaeozoic of Graz, GTN = Gurktal nappe, Kor = Koralpe, Sau = Saualpe, Ötz = Ötztal complex, Kr = Kreuzeck Mountains, Sch = Schobergruppe; LF = Lavanttal fault; SG = Sieggraben unit. The rectangle shows the location of Fig. 2.

metapelites of the Koralpe transect and discuss a range of long standing interpretations thereof.

GEOLOGICAL SETTING

The Koralpe region is one of two north–south trending ranges, which are interpreted as two eastward tilted blocks of the same sequence of Austroalpine nappes (Neubauer & Genser, 1990) (Figs 1 & 2). To the east, the Koralpe disappears beneath the Pannonian and Gosau basins, and to the south, it is truncated by the Lavanttal fault and Periadriatic lineament. To the west, it is juxtaposed against the Saualpe. To the north the eclogite and upper amphibolite facies Eo-Alpine rocks merge into the lower amphibolite facies rocks of the Gleinalpe complex (GC) (Becker, 1980) and, further north, into greenschist and subgreenschist facies rocks (Fig. 1). The Koralpe complex (KC) comprises a sequence of polymetamorphic micaschists and pelitic gneisses intercalated with marbles, amphibolites and eclogites plus abundant pegmatitic veins. At least three metamorphic overprints have been described in the literature, including Variscan, Permian and Cretaceous events (Frank *et al*., 1983; Schuster & Thöni, 1996; Schuster *et al*., 1999; Thöni, 1994; Miller & Thöni, 1997). Here, the pre-Cretaceous events are termed collectively as M1 (Schuster & Thöni, 1996; Schuster *et al*., 1999; Habler & Thöni, 2001) and the Cretaceous (Eo-Alpine) metamorphic event as M2.

The most important syn-M2 structural feature of the Koralpe is the Plattengneiss which is interpreted as an 800-m thick flat-lying ultramylonitic shear zone which covers substantial parts of the Koralpe region (Wimmer-Frey, 1984; Frank *et al*., 1983; Krohe, 1987; Weber, 1982; Jung, 1982). This deformation is part of the Cretaceous nappe stacking and led to penetrative deformation of all lithologies and occurred largely synchronous with the M2 paragenesis development. Because of the pervasive occurrence of this feature throughout the studied region, we refer to it as the *Plattengneiss event* and call it D2 to emphasize its occurrence at the time of M2. The patterns of quartz $<c>$ axes indicate top-to-the north displacement of the nappes during Eo-Alpine metamorphism (Krohe, 1987; Kurz *et al*., 2002). This northward thrusting formed a pronounced N–S trending stretching lineation (Fig. 3a). The N–S trending M2-lineation in the Koralpe is defined by garnet, muscovite, biotite, kyanite, plagioclase and quartz, which all show very clear features of syndeformational growth during high grade metamorphism (Fig. 3a). These features include garnet porphyroblasts elongated in the shear direction as well as dynamically recrystallized plagioclase porphyroclasts or garnet porphyroblasts with spiral inclusion trails (Fig. 4b).

After the Cretaceous M2 event, the flat-lying Koralpe was folded into open folds with E–W striking fold axes and wavelengths of several kilometres (Fig. 2b). In the south, the Koralpe is structurally overlain by the pre-Alpine Plankogel crystalline complex (PC) (Kurz *et al*., 2002). Further south, rocks of Eo-Alpine age continue into the Pohorje mountains (PM) (Hinterlechner-Ravnik *et al*., 1991).

Recognizing M2 parageneses

In summary, the M2 metamorphic event (which we are concerned with here) occurred synchronously with the principal structural fabric development of the region (the D2 Plattengneiss event). Here we rely on a range of geochronological studies that have shown that this M2/D2 event occurred in the Cretaceous (e.g. Thöni & Jagoutz, 1992, 1993) (Table 1). All previous metamorphic events are collectively referred to as M1.

However, it is not always easy to discriminate between the M2/D2 event and previous high grade events in the rock: Several studies have inferred that Eo-Alpine metamorphism was extremely short-lived (Ehlers *et al*., 1994) and dry (Frank *et al*., 1983), causing only partial equilibration of both geochronological and petrological systems, even in the highest grade parts of the transect (Thöni & Jagoutz, 1993). As a consequence M1 relics are found in most rocks. Fortunately, the M2 metamorphism gave rise to a distinctive new peak paragenesis which is usually easily distinguished on the basis of its syn-deformational growth within the D2 Plattengneiss fabric. This D2 deformation event has been related to the Cretaceous Eo-Alpine event by a number of authors (Frank *et al*., 1983; Wimmer-Frey, 1984; Krohe, 1987; Kurz *et al*., 2002). Also, the M2 mineral chemistries are distinctive and retrograde overprinting postdating M2 is minor, so M2 peak parageneses are generally well preserved (Fig. 4).

For an optimal comparison, only pelitic gneisses and schists were sampled, even in the northern most (Gleinalpe) parts of the transect, where metapelites only occur as minor intercalations in a predominantly orthogneiss sequence (Fig. 2). Because most of these metapelites are characterized by thermodynamically high variant assemblages (that are stable over a large *P-T* range), this approach allows us to compare very similar parageneses across the transect. Using this approach, several hundreds thin sections were studied and about 30 selected for the profile are discussed here.

PETROGRAPHY

The pelitic rock types shown in Fig. 2 are divided into two paragenetic groups. The first are pelitic mica-schists here called the 'micaschist type' and are abbreviated as MS and examples are shown in Fig. 4(a) (b) (c) and (d). The typical assemblage is Grt – Ms – Bt – Pl – Qtz, and it is this assemblage (in most cases also with Ky) that will be used throughout our *P-T* calculations. In Table 2, typical mica-schist assemblages containing this mineralogy are listed as MS1, MS2 and MS3. However, depending on bulk composition and metamorphic grade, mica-schists may be devoid of Bt or may contain Pg, St, Ky, Cld and/or Chl. In total, five different micaschist assemblages may be discerned (Table 2). The second rock type are pelitic gneisses containing the Eo-Alpine peak assemblage Grt + Ms + Bt + Pl + Ksp + Qtz + Ky. These rocks will be referred to

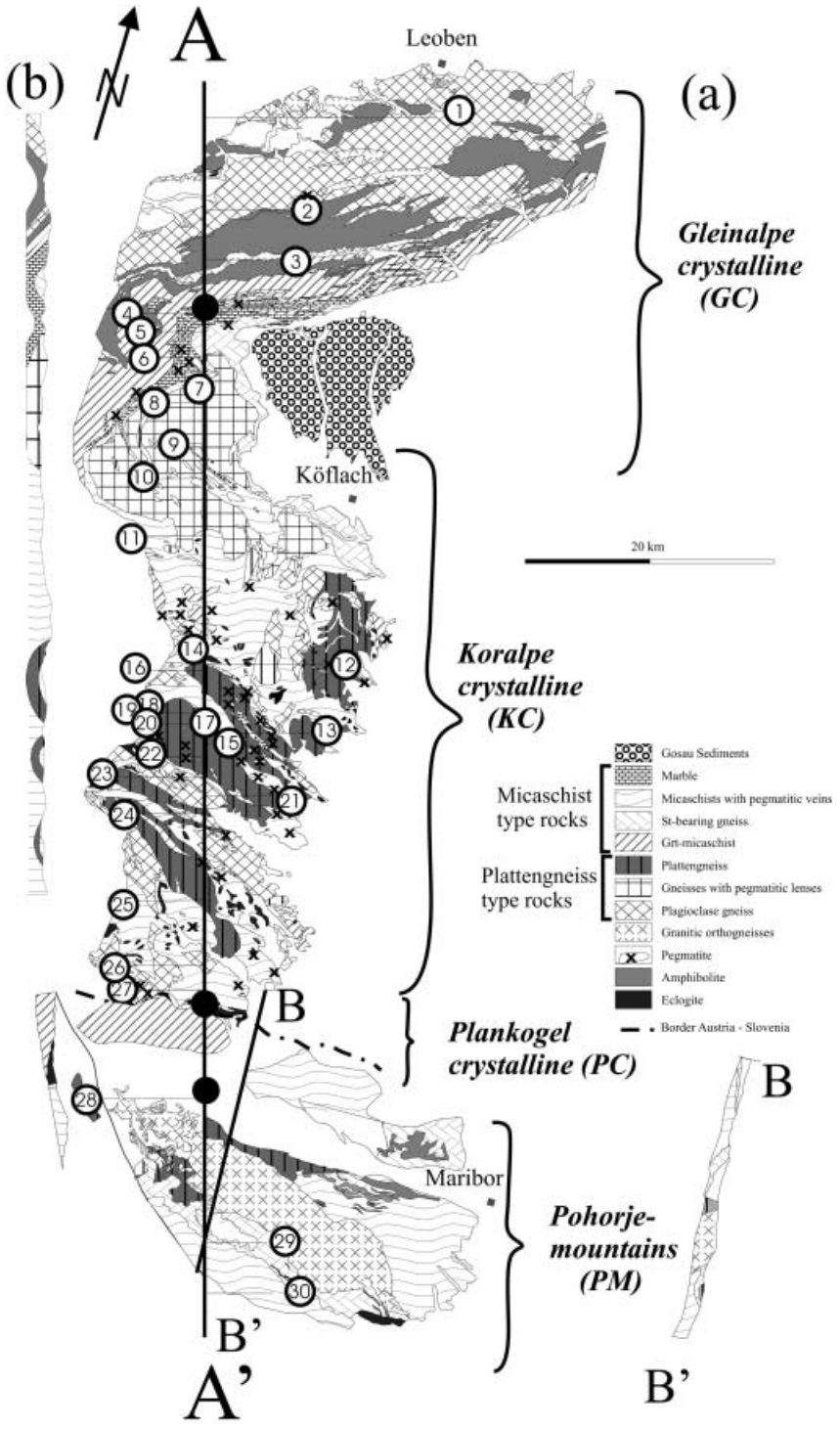

Fig. 2. (a) Geological map of the Koralpe region showing sample localities indicated by numbered circles (modified after Flügel & Neubauer, 1984 and Hinterlechner-Ravnik *et al.*, 1991). Samples 1–5, 14, 27, 29 and 30 contain micaschist assemblages; samples 6–13, 15–26 and 28 are Plattengneiss type rocks. Some inconsistencies between this division and the sample location according to the map legend arise from the close interfingering of different units on a scale that cannot be resolved on this map. The northern and southern margin of the map is defined by Tertiary faults, the eastern boundary is defined by the Pannonian basin and the western margin is the Styrian/Carinthian border. The thick line shows the projection line which is used for *P* and *T* profiles. The cross section B–B′ is modified after the geological map of Slovenia. (b) shows a profile along the projection line of the Koralpe and Gleinalpe crystalline rocks. The black dots on the projection line indicate the locations of major lithological contacts which have, in the past, been interpreted as major tectonic boundaries (Frank, 1987).

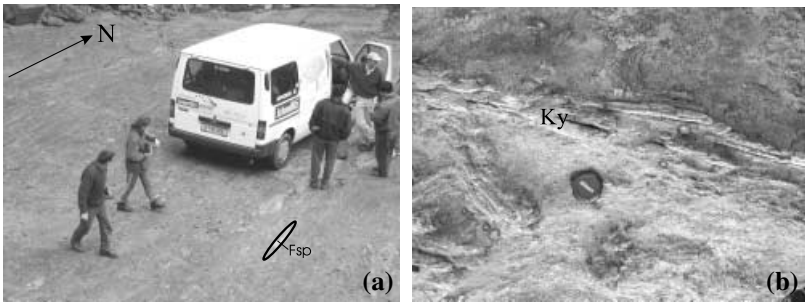

Fig. 3. (a) Field photograph of the Plattengneiss shear zone. The vehicle is parked on a foliation plane parallel to the stretching lineation. It may be seen that individual K-feldspar aggregates are elongated up to 1 m (N46°54.212′, E15°12.103′). (b) Micaschist type rocks (type 'Paramorphoseschiefer') showing kyanite paramorphs after chiastolite up to one metre in length (N46°46.875′, E14°58.415′).

as 'Plattengneiss type' and are abbreviated with PG, and are shown in Fig. 4(e) and (f). The micaschist type pelitic rocks occur predominantly in the northern part of the transect, known as Gleinalpe complex and in the southern part where they are known as the Plankogel crystalline complex. The Plattengneiss type rocks occur predominantly in the geographic and structural centre of the transect. Because of their distinct field appearance and geographic distribution, these two types are discussed separately.

Micaschist type rocks

Micaschists contain a pervasive D2 fabric which is not always pervasive enough to allow an unambiguous textural distinction between M1 and M2 garnet (Fig. 4c). Nevertheless, M2 garnet can be discerned on the basis of its chemistry (Fig. 5). M2 garnet porphyroblasts occur in all assemblages and vary in size between 0.5 mm and 10 mm. The crystals are rich in inclusions of quartz, paragonite, staurolite and occasionally chloritoid (Fig. 4b) which are preferentially located in crystal cores. Garnet porphyroblasts are partially replaced around their rims, mostly by biotite or chlorite (Fig. 4a,c). The least deformed rocks of the micaschist type occur in the south, where the garnet is inclusion free. White mica occurs in the D2 fabric as small crystals of muscovite mica fish that are occasionally intercalated with paragonite. The mica fish occasionally form a reaction texture from muscovite to chlorite and plagioclase in boudin necks. Biotite occurs in the D2 fabric or in pressure shadows around garnet (Fig. 4c). Static growth of mica occurred only in the southern part of the transect (Fig. 4d). Plagioclase porphyroclasts are often recrystallized at the rim. Staurolite either occurs as inclusions in garnet or as small grains of mm size in the matrix. Occasionally it also grows in shear bands in the vicinity of muscovite and kyanite. Larger staurolite porphyroclasts are partly replaced on the rim by muscovite. Kyanite is an abundant mineral in the micaschists, and varies in size from mm to metres (Fig. 3b).

Plattengneiss type rocks

There are two texturally different garnet generations in the Plattengneiss type rocks (Fig. 4e). The M1 garnet is inclusion free, 1–5 mm in size and often surrounded by small irregularly grown M2 garnet crystals on the rim. The M2 garnet is rich in inclusions of biotite, muscovite and quartz and partly replaced by biotite and kyanite (Fig. 4f). Muscovite occurs in the D2 fabric (often as coronas on kyanite) and as mica fish relics from M1. The M2 muscovite replaced plagioclase in the deformation twins. Biotite preferentially grew in the pressure shadows around garnet or between small syntectonic garnet porphyroblasts and also occurs as inclusions in garnet. Feldspar porphyroblasts (both, K-feldspar and plagioclase) occur in the Plattengneiss and are highly strained and elongated to the metre scale (Fig. 3a). These porphyroblasts show textures of dynamic recrystallization (core–mantle structures) with long tails of recrystallized grains. Elongated kyanite aggregates (Fig. 4e) commonly occur and are interpreted as deformed equivalents of the large kyanite porphyroblasts shown in Fig. 3(b).

MINERAL CHEMISTRY

Analytical conditions

All electron microprobe analyses were carried out with a wavelength-dispersive JEOL JXA 8600 system at the Department of Earth Sciences at the University of Bristol with operating conditions of 15 kV and 20 nA beam current and a SEM JEOL JSM-6310 at the Department of Mineralogy and Petrology at the University of Graz with operating conditions of 15 kV and 5 nA beam current. Natural and synthetic silicates and oxides were used for calibration. The mineral formulae were calculated with the program AX (Holland 1999, http://www.esc.cam.ac.uk/astaff/holland). The formulae were normalized to oxygen basis and Fe^{2+}/Fe^{3+} was calculated according to charge balance considerations. Representative microprobe analyses can be found in Table 3.

Micaschist type rocks

Different types of garnet have been distinguished in micaschists (Fig. 5a–c). Garnet that grew only during M2 (Fig. 5a), some that grew almost exclusively during M1 (Fig. 5b) and some that grew during both events. Zoning within M2 parts of garnet is not very strong. As shown in Fig. 5(a), X_{Alm} decreases from 0.72 to 0.62 from core to rim and X_{Grs} from 0.20 to 0.10 while X_{Sps} continuously 0.00 from core to rim. The X_{Prp} increases from 0.14 to 0.30 from core to rim. Note that there is very little retrograde zoning, which is in part due to the large grain sizes depicted here. In contrast, M1 garnet in the mica-schists has strongly zoned profiles but will not be discussed in further detail as it is not used in this study.

White mica in the micaschist type rocks consists of muscovite and paragonite. Muscovite occurs as mica fish and as lineation-forming aggregates of small crystals in the matrix. Mica fish are zoned with increasing Si content from 3.10 (core) to 3.30 a.p.f.u. (rim). Matrix muscovite is often intercalated with paragonite and has a Si content of 3.32 a.p.f.u. Both mica fish and matrix muscovite also contain some margarite component.

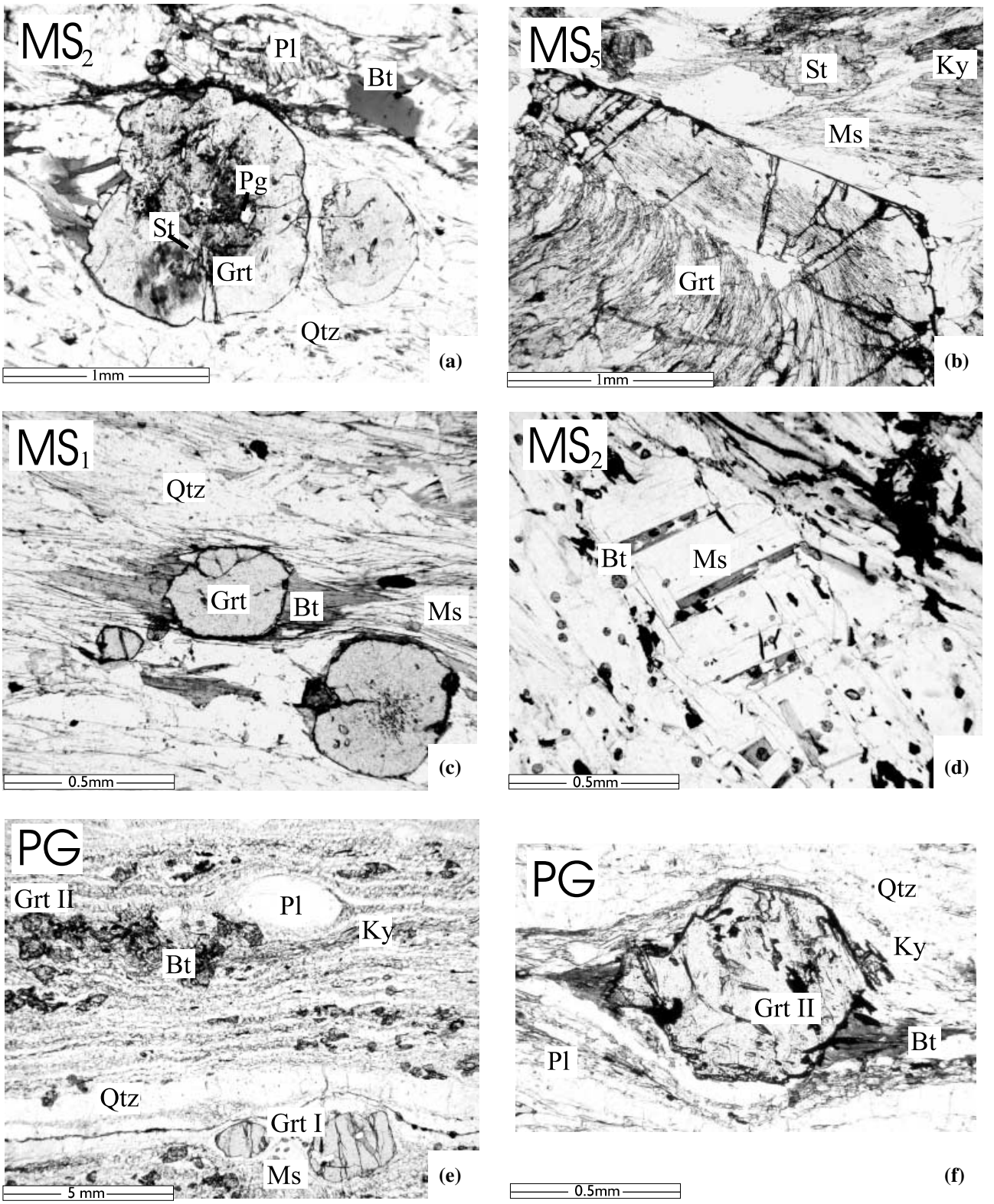

Fig. 4. Representative photomicrographs of characteristic textures of the Koralpe transect (mineral abbreviations after Kretz, 1983). (a) (b) (c) and (d) are examples from the micaschist type rocks; (e) and (f) from the Plattengneiss type rocks. Note that the biotite growth in pressure shadows of garnet (f) is the only retrograde reaction that may be observed in the Plattengneiss. Late growth of biotite may also be observed in (d). Also not the syn-deformationally grown and broken (but not retrogressed) M2 garnet in (e). Detailed descriptions are given in text.

Table 1. Summary of geochronological data from the Koralpe and surrounding regions. For details of the regional names see References given on Fig. 2.

Rock unit	Age	Reference
Sieggraben unit:		
eclogite	Neubauer *et al.* (1999)	136.1 ± 0.5 Ma and 108.2 ± 0.3 Ma (Ar-Ar cooling ages from the Hbl crystals. Variation due to compositional variation.
Gleinalpe complex:		
granite gneiss and pegmatite (Humpelgraben)	Neubauer *et al.*, 1995	94.1 ± 1.4 (Ar/Ar Hbl) cooling age 84.3 ± 0.7 (Ar/Ar Ms) 87.6 ± 0.6 (Ar/Ar Ms)
orthogneiss boulders	Neubauer (1987)	139.5 Ma (U/Pb-Zircon) – Eoalpine peak
	Dallmeyer *et al.* (1996)	84.3 ± 0.7–88.4 ± 0.5 (Ar/Ar Ms) 95.4 ± 1.2 (Ar/Ar Hbl)
Plattengneiss	Frank *et al.* (1983)	K/Ar: Ms: 75–100 Ma; Bt: 75–100 Ma
Koralm basis (Wolfsberger unit)	age based on Jung (1982)	Ms from pegmatites: 75–100 Ma; Rb/Sr: Ms: 75–120 Ma; Bt: 70–100 Ma; Ms aus Peg: > 200 Ma
Amphibolites (Speikkomplex)	Frank, 2001 pers. comm. new data from the samples from Jung (1982) unpublished	Ar-Ar Hbl plateau ages represent Eoalpine crystallization Ar-Ar White mica ages show steps in the profiles, indication late stage normal faulting of the upper nappes of the Koralpe NO Variscan or Permian Ages at all
Gaberl, locality 'Märchenwiese'	Frank *et al.* (1983)	Ar-Ar Ms cooling age ~80 Ma (based on samples from Jung, 1982) Ar-Ar Hbl 95–107 Ma (samples from Jung, 1982)
Speik Complex		
Koralpe complex:		
relic gabbro	Thöni & Jagoutz (1992)	275 ± 18 Ma (Sm-Nd isochron)
eclogites	Thöni & Jagoutz (1993)	93 ± 15 Ma (Sm-Nd isochron)
	Thöni (1999)	92.5 ± 1 Ma (Rb-Sr whole rock); 100 Ma (Rb-Sr Grt-Cpx); 89.8 ± 2.6 Ma (Sm-Nd)
eclogite host rocks (Saualpe)		90.7 ± 3.6 Ma (Sm-Nd); 90.3 ± 1 Ma (Rb-Sr, Ms-Grt)
eclogites	Thöni & Miller (1996)	88.5 ± 1.7, 90.9 ± 0.7 94.0 ± 2.7 (Sm-Nd)
pegmatite		Grt from pegmatite mylonite from the PG (Stainz, Rachling): 256 ± 1 Ma, 264 ± 1 Ma (Sm-Nd)
Li-pegmatites	Thöni & Miller, 2000	WR-Spd: 238.5 ± 2.2 Ma, 242.8 ± 1.7 Ma Rb-Sr WR: 245 ± 20 Ma 225 ± 3, 222 ± 8 Ma
Li-free pegmatites		(183 ± 3 Ma – younger Grt overgrows older) (Sm-Nd) Rb-Sr WR: 245 ± 20 Ma Rb-Sr WR: 265 ± 170 Ma
aplitic border zone		87.5 ± 5.2 Ma (Eoalpine peak) 65.9 ± 1.3 Ma ('mixed' age – later and earlier Eoalpine component)
Wolfsberg granite		87.9 ± 4.7 Ma (intense metamorphic overprint)
Wolfsberg granite	Morauf (1980)	Rb-Sr: 258 ± 11 Ma, Eoalpine overprint: White mica: Rb-Sr: 79–80 ± 3Ma; K-Ar: 75–78 ± 3Ma; Bt: Rb-Sr: 77–73 ± 3Ma; K-Ar: 80 ± 3Ma;
Pegmatites	Morauf (1981)	Ms I: 240–265 Ma Ms II: 72–122 Ma
Li pegmatite	Heede (1997)	U/Pb Zircon multigrain
Pegmatites related to eclogites (Saualpe)		240 ± 1.5 Ma Cretaceous ages (pegmatite related to eclogite U/Pb Zircon)
Metapelite–eclogite host	Paquette & Gebauer (1991)	U/Pb magmatic zircon: 299 ± 11 Ma
Plankogel complex:		
Metapelite	Lichem *et al.* (1997)	Grt cores, 285 ± 1 Ma
Metapelite	Thöni (2002)	Grt cores: 263.5 ± 6.8 Ma
Pohorje mountains:		
Metapelite	Thöni (2002)	93 ± 1.8 Ma Sm-Nd Grt-whole rock
Gneiss		87 ± 3.1 Ma Sm-Nd Grt-whole rock

M2 biotite in the micaschist rock types occurs in both locations, in pressure shadows around garnet and as inclusions in M2 garnet and is homogeneous in composition with X_{Mg} of around 0.60 (Table 3). TiO_2 content of biotite is generally around 1.70 wt%.

Plagioclase occurs as part of the coarse grained M2 paragenesis in some of the micaschist type rocks (Table 2) and is typically zoned, where X_{Ab} varies from 0.70 to 0.90 from core to rim.

Staurolite varies substantially between different parageneses. Staurolite in assemblage MS5 varies in X_{Mg} between 0.17 and 0.19 and has low ZnO contents of about 1 wt% but increases locally to 4 wt% in inclusions. In assemblage MS4, staurolite has higher X_{Mg} of 0.20–0.25 and ZnO of 2.0 wt%. The matrix staurolite of MS_3 has 0.30 wt% ZnO and X_{Mg} of 0.25. Staurolite located in narrow shear bands has X_{Mg} of 0.20 and low ZnO contents (1.70 wt%).

Table 2. Observed mineral assemblages of the metapelites of the Koralpe. All assemblages have Rt and Ilm as accessories and Qtz in excess. Note that these assemblages are not necessarily the M2 equilibrium assemblage used for the thermobarometric calculations (Table 4), but is a complete list of minerals observed in thin section. For details on textural relationships between different phases see text. The two shaded assemblages are those not used for thermobarometric calculations.

Assemblage	Grt	Ms	Pg	Bt	Pl	Ky	Kfs	St	Chl	Cld
MS_1	+	+	+	+	+ –	–	–	–	+	–
MS_2	+	+	+	+	+	+	–	+ –	+	–
MS_3	+	+	–	+	–	+	–	+ –	+ –	–
MS_4	+	+	–	–	+	+	–	+ –	+ –	–
MS_5	+	+	–	–	–	+	–	+ –	+ –	+ –
PG	+	+	–	+	+	+	+ –	+ –	+ –	+ –

Plattengneiss type rocks

The M2 garnet larger than 1 mm has prograde zonation with increasing Ca and Mg and decrease in Fe from core to rim and low Mn contents (rim composition: $X_{Grs} = 0.15$, $X_{Prp} = 0.25$, $X_{Alm} = 0.59$). Although very small garnet shows diffusive zoning profiles, no textural evidence for retrogression is found in the Plattengneiss. This is consistent with results of Ehlers *et al.* (1994). M2 rims on M1 garnet are usually easily recognized by much higher values of X_{Grs} and lower X_{Sps}, X_{Alm} and X_{Prp} (Figs 5d,e & 6a). The transition from M1 to M2 garnet can be sharp (as in Fig. 5c,d) or continuous (as in Fig. 5f). The M1 garnet generation in a typical Plattengneiss can be distinguished not only texturally (Fig. 4e), but also chemically on the basis of a higher Mn content (X_{Sps} *c.* 0.08) (Fig. 5c–f).

In the Plattengneiss there is only one mica, named as muscovite even though it contains a higher phengite component than the micaschist muscovite. It occurs in at least three textural and chemical varieties (see above, Fig. 6c). The Si content of white mica in the Plattengneiss is between 3.01 and 3.32 a.p.f.u. The cores of mica fish have the lowest phengite content (preserved from the M1 event), while the rims have higher contents. Mica inclusions in M2 garnet and small mica needles in the matrix coexisting with plagioclase (as outlined in Fig. 6b) have the highest Si of 3.32 a.p.f.u.

M2 biotite shows X_{Mg} between 0.60 and 0.75. Depending on the textural position of the biotite the TiO_2 contents vary between 0.35 wt% where it is in the pressure shadows and 4.50–5.50 wt% in inclusions in M2 garnet.

Cores of plagioclase porphyroblasts are generally anorthite rich, while rims and matrix (which consists

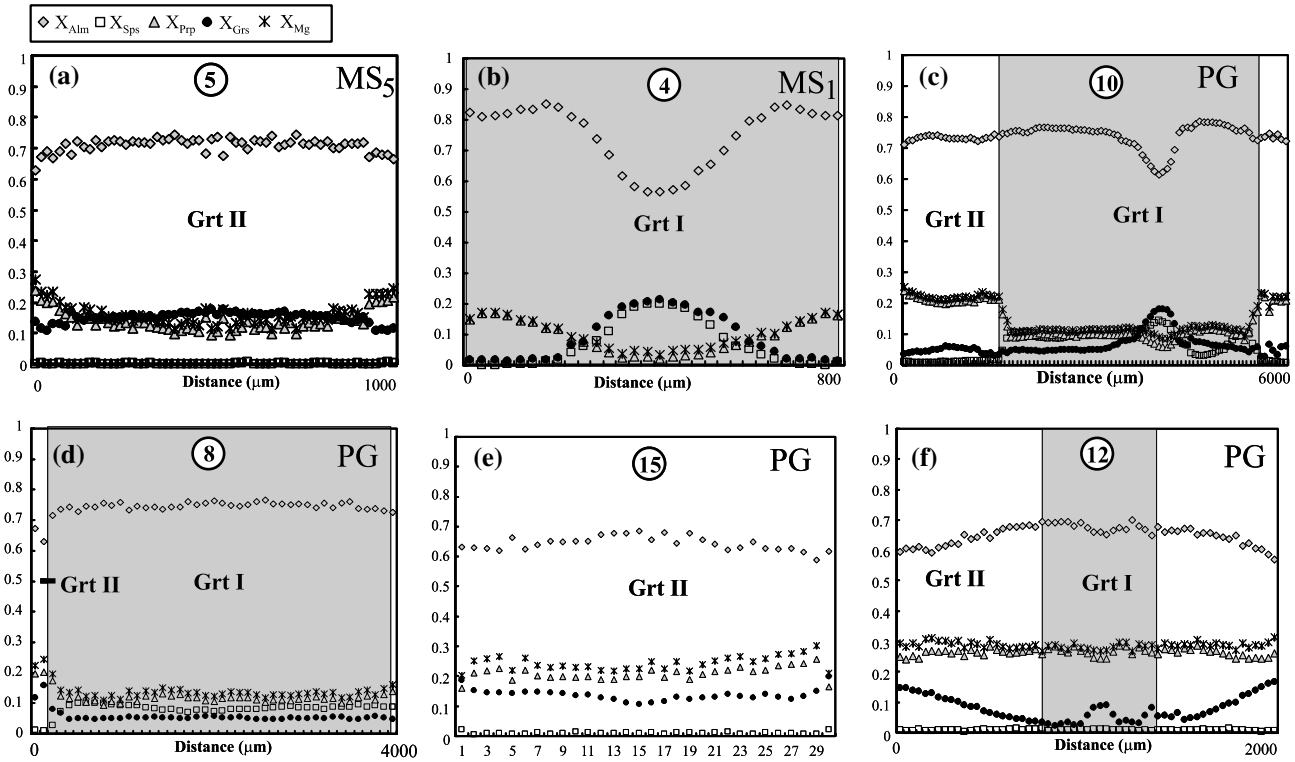

Fig. 5. Representative garnet zoning profiles from the Koralpe transect. (a) and (b) are from the micaschist type rocks (MS). (c), (d), (e), and (f) from the Plattengneiss type rocks (PG). Garnet I (garnet that grew during M1) is shaded grey; Garnet II (that grew during M2) is left white. Numbers in circles refer to the sample numbers from Fig. 2. Note that the zoning profiles of some garnet I (e.g. that in (b) or (c)) indicate that the rocks may have had a complicated metamorphic history prior to M2.

Table 3. Microprobe analyses of representative minerals. Mineral abbreviations used are after Kretz (1983). Sample numbers correspond to those on Fig. 2 and their assignment to mica-schists or Plattengneiss type rocks is according to the caption of Fig. 2. Mineral formulae calculations were performed using AX.
(a). Representative electron microprobe analyses of garnet[1] (all rim compositions).

Sample	1	4	6	8	11	12	14	15	16	17
SiO_2	37.82	36.59	38.42	39.04	37.81	38.48	38.09	38.37	38.10	38.87
TiO_2	0.00	0.05	0.07	0.14	n.d.	n.d.	0.08	0.20	0.14	0.00
Al_2O_3	21.68	20.52	21.27	21.60	21.49	21.47	21.54	21.52	20.90	21.71
Cr_2O_3	n.d.	n.d.	n.d.	n.d.	n.d.	n.d.	n.d.	n.d.	n.d.	0.00
Fe_2O_3	0.23	< 0.01	n.d.	n.d.	n.d.	n.d.	n.d.	n.d.	n.d.	0.00
FeO	30.52	37.75	30.02	27.25	30.92	28.97	31.14	28.78	30.46	26.93
MnO	0.16	0.08	0.29	0.25	0.95	0.73	0.76	0.27	0.48	0.00
MgO	3.83	3.25	3.60	5.31	5.44	6.23	6.05	5.42	4.71	6.63
CaO	6.02	0.77	6.68	7.23	2.71	4.06	2.28	5.47	4.99	5.00
Σ	100.26	99.01	100.35	100.82	99.32	99.94	99.94	100.03	99.78	99.14
Si	2.98	2.99	3.02	3.02	2.97	3.00	2.98	3.00	3.01	3.03
Ti	< 0.01	< 0.01	< 0.01	< 0.01	n.d.	n.d.	< 0.01	0.01	< 0.01	n.d.
Al	2.02	1.98	1.97	1.97	1.99	1.97	1.99	1.99	1.95	2.00
Cr	0.00	n.d.	n.d.	n.d.	0.07	n.d.	n.d.	n.d.	n.d.	n.d.
Fe^{3+}	0.01	< 0.01	n.d.	n.d.	0.07	n.d.	n.d.	n.d.	n.d.	n.d.
Fe^{2+}	2.01	2.58	1.98	1.76	2.03	1.89	2.04	1.88	2.02	1.76
Mn	0.01	0.01	0.02	0.02	0.06	0.05	0.05	0.02	0.03	0.00
Mg	0.45	0.40	0.42	0.61	0.64	0.72	0.71	0.63	0.56	0.77
Ca	0.51	0.07	0.56	0.60	0.23	0.34	0.19	0.46	0.42	0.42
Σ cations	8.00	8.01	7.98	7.98	7.99	7.96	7.96	7.99	7.99	7.97
X_{Alm}	0.67	0.85	0.66	0.59	0.69	0.63	0.68	0.63	0.67	0.60
X_{Prp}	0.15	0.13	0.14	0.20	0.22	0.24	0.24	0.21	0.18	0.26
X_{Grs}	0.17	0.02	0.19	0.20	0.08	0.11	0.06	0.15	0.14	0.14
X_{Sps}	< 0.01	< 0.01	0.01	0.01	0.02	0.02	0.02	0.01	0.01	< 0.01

[1] Formulae normalized to 12 oxygen; n.d., not detected, X_{Alm}: [Fe/(Fe + Mg + Ca + Mn)], X_{Prp}: [Mg/(Fe + Mg + Ca + Mn)], X_{Grs}: [Ca/(Fe + Mg + Ca + Mn)], X_{Sps}: [Mn/(Fe + Mg + Ca + Mn)], n.d. not detected. Here only rim compositions are shown, which have been used for the *PT* calculations. The composition from the cores can be seen in the garnet profiles in Fig. 5.

Table 3(b). Representative electron microprobe analyses of white mica[2] (muscovite and paragonite).

Sample	1(Ms)	4(Ms)	6(Ms)	8(Ms)	11(Ms)	12(Ms)	14 (Pg)	15(Ms)	16(Ms)	17(Ms)
SiO_2	48.72	45.73	46.83	49.01	49.96	47.97	46.12	46.50	48.45	50.08
TiO_2	0.52	0.36	0.69	1.37	1.04	1.57	0.11	1.98	0.40	1.80
Al_2O_3	33.51	35.10	32.94	31.82	31.05	31.73	40.72	29.80	32.88	31.76
Cr_2O_3	n.d.	n.d.	n.d.	n.d.	n.d.	n.d.	n.d.	n.d.	n.d.	n.d.
Fe_2O_3	n.d.	2.75	n.d.	n.d.	0.07	0.66	n.d.	0.74	0.01	n.d.
FeO	1.19	1.23	1.42	1.49	1.47	1.24	0.64	1.44	1.61	1.33
MnO	n.d.	n.d.	0.09	n.d.	0.06	n.d.	0.00	0.00	0.02	n.d.
MgO	1.44	0.82	1.57	2.15	2.39	1.87	0.31	2.23	1.89	2.27
CaO	n.d.	n.d.	0.05	n.d.	n.d.	n.d.	1.03	0.00	0.06	n.d.
Na_2O	0.74	1.83	1.44	0.77	0.46	0.21	7.02	0.27	0.35	0.21
K_2O	9.48	8.48	9.05	9.64	9.32	9.38	0.18	10.98	9.84	10.06
Σ	95.60	96.30	94.08	96.25	95.82	94.63	96.13	93.94	95.51	97.51
Si	3.20	3.02	3.15	3.22	3.28	3.19	2.93	3.17	3.20	3.24
Ti	0.03	0.02	0.04	0.07	0.05	0.08	0.01	0.10	0.02	0.09
$Al^{IV.}$	0.80	0.98	0.86	0.79	0.72	0.81	1.08	0.83	0.80	0.76
$Al^{VI.}$	1.80	1.75	1.75	1.68	1.68	1.69	1.97	1.57	1.76	1.66
Cr	n.d.	n.d.	n.d.	n.d.	n.d.	n.d.	n.d.	n.d.	n.d.	n.d.
Fe^{3+}	n.d.	0.14	n.d.	n.d.	0.00	0.03	n.d.	0.04	n.d.	n.d.
Fe^{2+}	0.07	0.07	0.08	0.08	0.08	0.07	0.03	0.08	0.09	0.07
Mn	n.d.	n.d.	0.01	0.00	0.00	n.d.	n.d.	n.d.	< 0.01	n.d.
Mg	0.14	0.08	0.16	0.21	0.23	0.19	0.03	0.23	0.19	0.22
Ca	n.d.	n.d.	< 0.01	n.d.	n.d.	n.d.	0.07	n.d.	< 0.01	n.d.
Na	0.09	0.24	0.19	0.10	0.06	0.03	0.86	0.04	0.05	0.03
K	0.80	0.72	0.78	0.81	0.78	0.80	0.02	0.96	0.83	0.83
S	6.92	7.00	6.99	6.94	6.89	6.88	6.99	7.01	6.93	6.89

[2] Formulae normalized to to 11 oxygen.

Table 3(c). Representative electron microprobe analyses of biotite[3].

Sample	2	4	6	8	11	12	14	15	16	17
SiO_2	36.59	35.74	37.30	37.84	36.74	36.75	37.23	36.71	37.28	37.03
TiO_2	1.99	1.23	1.78	1.92	2.17	3.62	1.55	4.04	3.63	3.25
Al_2O_3	18.36	18.31	17.40	18.73	18.22	17.20	18.78	18.09	18.15	19.04
Cr_2O_3	n.d.	0.03	n.d.	n.d.	n.d.	n.d.	n.d.	n.d.	n.d.	n.d.
Fe_2O_3	n.d.	2.75	n.d.	n.d.	n.d.	0.66	1.98	0.74	0.07	n.d.
FeO	15.14	18.05	16.58	14.51	15.30	13.65	12.73	14.16	16.29	14.44
MnO	0.05	n.d.	0.15	n.d.	n.d.	n.d.	0.05	0.00	0.04	n.d.

Table 3(c). (*Cont'd*).

Sample	2	4	6	8	11	12	14	15	16	17
MgO	12.71	10.65	12.03	13.32	12.29	12.82	14.30	11.69	10.97	12.55
CaO	0.03	0.02	0.04	0.04	0.07	0.00	0.12	0.13	0.02	n.d.
Na_2O	0.11	0.26	0.18	0.30	0.79	0.06	0.32	n.d.	0.10	0.10
K_2O	9.93	8.00	8.55	8.41	8.97	9.71	8.18	9.84	9.31	9.24
Σ	94.91	95.04	94.01	95.07	94.55	94.47	95.24	95.40	95.86	95.65
Si	2.74	2.71	2.82	2.79	2.76	2.75	2.73	2.73	2.77	2.73
Ti	0.11	0.07	0.10	0.11	0.12	0.20	0.09	0.23	0.20	0.18
$Al^{IV.}$	1.26	1.29	1.18	1.21	1.24	1.25	1.27	1.27	1.24	1.27
$Al^{VI.}$	0.37	0.34	0.37	0.41	0.37	0.27	0.36	0.31	0.35	0.38
Cr	0.00	0.00	0.00	n.d.	n.d.	n.d.	n.d.	n.d.	n.d.	n.d.
Fe^{3+}	0.00	0.16	0.00	n.d.	n.d.	0.04	0.11	0.04	< 0.01	n.d.
Fe^{2+}	0.95	1.14	1.05	0.89	0.96	0.86	0.78	0.88	1.01	0.89
Mn	0.00	n.d.	0.01	n.d.	n.d.	n.d.	< 0.01	n.d.	0.00	n.d.
Mg	1.42	1.20	1.35	1.46	1.37	1.43	1.56	1.30	1.21	1.38
Ca	< 0.01	< 0.01	< 0.01	< 0.01	< 0.01	n.d.	0.01	0.01	< 0.01	n.d.
Na	0.02	0.04	0.03	0.04	0.12	< 0.01	0.05	n.d.	0.02	0.01
K	0.95	0.77	0.82	0.79	0.86	0.93	0.77	0.93	0.88	0.87
Σ	7.82	7.73	7.73	7.71	7.80	7.73	7.72	7.70	7.68	7.71

[3] Formulae normalized to to 11 oxygen.

Table 3(d). Representative electron microprobe analyses of plagioclase[4].

Sample	1	3	6	8	11	12	14	15	16	17
SiO_2	65.99	67.18	63.03	65.91	65.96	66.58	65.63	65.63	67.24	65.86
Al_2O_3	20.33	21.40	23.39	21.97	21.05	21.31	22.43	21.67	20.47	21.70
Fe_2O_3	n.d.	n.d.	0.12	0.07	0.22	n.d.	n.d.	0.09	n.d.	0.00
FeO	n.d.	n.d.	n.d.	n.d.	n.d.	n.d.	n.d.	n.d.	n.d.	0.00
MgO	n.d.	n.d.	n.d.	n.d.	n.d.	n.d.	0.09	n.d.	n.d.	0.00
CaO	3.41	1.92	4.67	2.78	2.29	2.01	3.35	2.43	1.68	3.01
Na_2O	10.93	10.78	9.28	9.88	10.83	9.99	10.11	9.62	9.96	9.38
K_2O	0.07	0.06	0.11	0.11	0.05	0.12	0.07	0.11	0.10	0.21
Σ	100.73	101.34	100.60	100.72	100.40	100.01	101.68	99.55	99.45	100.16
Si	2.90	2.91	2.77	2.87	2.89	2.92	2.84	2.89	2.95	2.89
Al	1.05	1.09	1.21	1.13	1.09	1.10	1.15	1.13	1.06	1.12
Fe^{3+}	n.d.	n.d.	0.00	0.00	0.01	n.d.	n.d.	0.00	n.d.	0.00
Fe^{2+}	n.d.	n.d.	n.d.	n.d.	n.d.	n.d.	n.d.	n.d.	n.d.	0.00
Mg	n.d.	n.d.	n.d.	n.d.	n.d.	n.d.	0.01	n.d.	n.d.	0.00
Ca	0.16	0.09	0.22	0.13	0.11	0.09	0.16	0.11	0.08	0.14
Na	0.93	0.91	0.79	0.84	0.92	0.85	0.85	0.82	0.85	0.80
K	0.00	0.00	0.01	0.01	0.00	0.01	0.00	0.01	0.01	0.01
Σ	5.04	5.00	5.01	4.97	5.02	4.96	5.01	4.96	4.95	4.96
X_{Ab}	0.85	0.91	0.78	0.86	0.89	0.89	0.84	0.87	0.91	0.84
X_{An}	0.15	0.09	0.22	0.13	0.10	0.10	0.15	0.12	0.08	0.15
X_{Ksp}	0.00	0.00	0.01	0.01	0.00	0.01	0.00	0.01	0.01	0.01

[4] Mineral formulae normalised to 8 cations. $X_{Ab} = [Na/(Na + Ca + K)]$; $X_{An} = [Ca/(Na + Ca + K)]$; $X_{Ksp} = [K/(Na + Ca + K)]$.

Table 3(e). Representative electron microprobe analyses of staurolite and chloritoid.

Sample	3(St)	5(St)	14(St)	31(St)	27(St)	26(St)	30(St)	29(St)	5(Cld)
SiO_2	27.58	28.16	28.11	28.15	28.27	28.63	28.61	28.15	24.31
TiO_2	0.69	0.58	0.51	0.52	0.56	0.34	0.50	0.51	n.d.
Al_2O_3	54.10	52.15	52.86	53.25	53.86	53.70	52.65	51.59	39.77
Cr_2O_3	0.07	n.d.	n.d.	n.d.	0.08	n.d.	n.d.	n.d.	n.d.
Fe_2O_3	n.d.	n.d.	n.d.	n.d.	n.d.	n.d.	n.d.	n.d.	n.d.
FeO	12.60	12.06	10.28	13.66	13.88	11.96	13.27	10.36	23.31
MnO	0.16	0.03	0.10	0.29	0.03	0.11	0.27	0.19	0.16
MgO	1.49	1.89	2.14	1.44	1.38	2.08	1.82	1.86	2.79
CaO	n.d.	0.02	n.d.	n.d.	0.00	0.03	0.06	0.03	0.08
Na_2O	0.08	0.07	0.15	0.18	n.d.	0.07	0.36	1.03	0.01
K_2O	n.d.	n.d.	0.05	n.d.	0.01	0.01	n.d.	0.01	0.06
ZnO	1.08	2.39	3.55	0.75	0.31	1.69	0.62	2.23	n.d.
Σ	97.85	97.35	97.75	98.24	98.38	98.62	98.16	95.96	90.49
Si	7.69	7.99	7.96	7.84	7.82	7.93	7.95	8.05	1.02
Ti	0.15	0.11	0.11	0.11	0.12	0.07	0.10	0.11	0.00
Al	17.79	17.45	17.64	17.48	17.55	17.54	17.25	17.39	1.97
Cr	0.02	n.d.	n.d.	n.d.	0.02	n.d.	n.d.	n.d.	n.d.
Fe^{3+}	n.d.	n.d.	n.d.	n.d.	n.d.	n.d.	n.d.	n.d.	n.d.
Fe^{2+}	2.94	2.77	2.43	3.18	3.21	2.77	3.08	2.48	0.82
Mn	0.04	n.d.	0.02	0.07	0.01	0.03	0.06	0.05	0.01
Mg	0.62	0.83	0.91	0.60	0.57	0.86	0.75	0.79	0.17
Ca	0.00	n.d.	n.d.	n.d.	n.d.	0.01	0.02	0.01	0.00
Na	0.05	0.05	0.08	0.10	n.d.	0.04	0.19	0.57	0.00
K	n.d.	n.d.	0.02	n.d.	< 0.01	< 0.01	n.d.	< 0.01	< 0.01
Σ	29.28	29.20	29.17	29.36	29.28	29.25	29.42	29.44	3.99

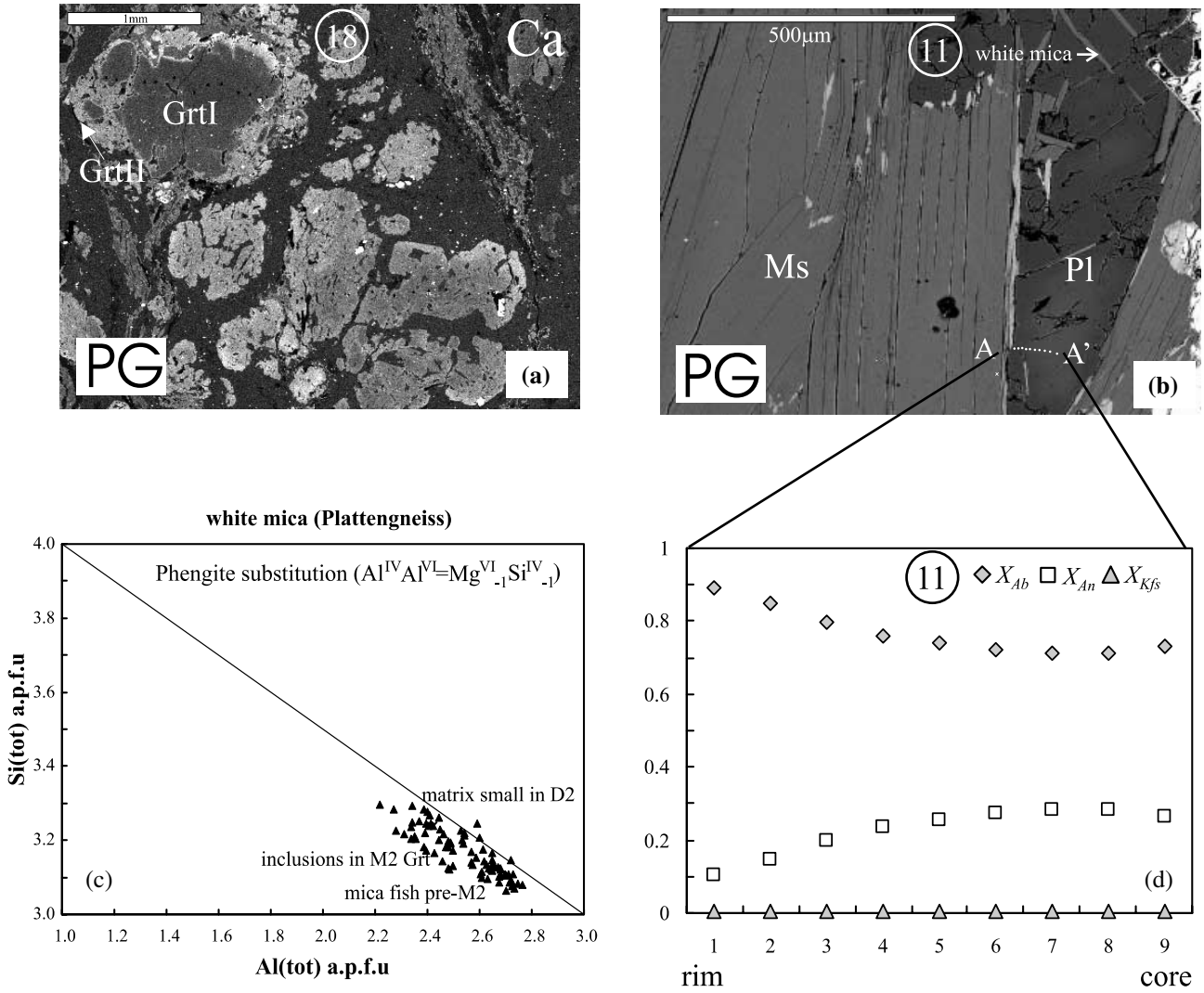

Fig. 6. Mineral chemistry of some representative Plattengneiss samples (PG). Sample numbers in white circles correspond to those shown in Fig. 2. (a) Ca-distribution X-ray map of M1 and M2 garnet. (dark is low Ca, light shading is high Ca). (b) Backscattered SE image of plagioclase – muscovite interrelationships. The compositional changes along profile A-A′ are shown in (d). (c) White mica chemistry. (d) Plagioclase zoning profile from (b).

of highly strained recrystallized aggregates of the porphyroblast rims) are more albite rich. However a compositional variation larger than $X_{An} = 0.09$–0.30 is rarely exceeded. A representative profile of a plagioclase of assemblage PG is shown in Fig. 6(b, d).

GEOTHERMOBAROMETRY

Approach and numerical technique

Here we concentrate on the Eo-Alpine M2 metamorphic event and so thermobarometric calculations relate to the M2 assemblages. Because of the lack of retrograde overprint (see above) it is straight forward to extract M2 peak conditions from M2 parageneses. In order to be able to compare the thermobarometric calculations for all samples of the transect, only M2 minerals present in all samples are used. For most samples, this is the assemblage Grt–Ms–Bt–Pl–Ky which is used for thermobarometric calculations with THERMOCALC version 2.7 of Powell & Holland (1988) and the thermodynamic data set of Holland & Powell (1998). However, there is one exception, which is assemblage MS1 which does not contain kyanite (Table 2), but plays an important role in the profile as it is the assemblage of the northernmost sample. Due to the absence of kyanite in this sample, all end-members of this assemblage were used all in order to obtain enough independent reactions to undertake average *PT* calculations with THERMOCALC. In all other samples the mica end-members celadonite and eastonite were omitted as they increase the error on the calculations, but do not change the actual results. This was checked

by performing both calculations including and excluding these two end-members.

The mineral activities were calculated with AX. To optimize the result a three-step procedure was used. (1) An iteration was applied between (i) activity calculation (using a guess for P and T for the first iteration only) and (ii) calculations of the P-T conditions of the stable intersections of reactions between these end-members using these activities (using 'mode 1' of THERMOCALC). For these iterations we used H_2O absent intersections as the water activities are as yet unknown (these are the reactions with superscript 1 on Table 5). This procedure was performed until changes between iterations are small. (2) The water activities were calculated using the P–T estimates from the previous procedure. This was done using 'mode 3' of THERMOCALC. 3) The optimized activities of both mineral end members and H_2O were used as input of the average PT mode in THERMOCALC ('mode 2') to derive formation conditions of the assemblages. Finally, we neglected P–T results obtained with this procedure that had large errors, and retained a final set of 28 data points along the transect. These final results of the stepwise calculations are shown in Table 4. The sets of mineral reactions, which were used for these calculations are shown for the three assemblages in Table 5.

To provide an independent constraint, the THERMOCALC results were compared against thermobarometric calculations using WEBINVEQ (Gordon, 1998), which is based on the data set of Berman (1988). In order to perform this independent comparison, all mineral activities were recalculated with activity models compatible with TWQ 1.02 (http://ichor.geo.ucalgary.ca/~tmg/Webinveq/rgb95.html).

Results

The thermobarometric results obtained from the optimized THERMOCALC calculations are presented in Fig. 7 and Table 4. In this figure, our results were supplemented with a summary of most available data from the literature (Gregurek *et al.*, 1997; Miller & Thöni, 1997; Ehlers *et al.*, 1994; Stüwe & Ehlers, 1996). All data points are constrained to 1 σ errors smaller than 1.6 kbar and < 68 °C for peak temperature (Fig. 7). The data shown in Fig. 7 are those for the H_2O invariant points shown in Table 4 in the third column. As the exact H_2O activities of the Koralpe rocks are uncertain, we believe that it is safer to use these results than those of the average PT calculations performed with THERMOCALC or WEBINVEQ (shown in the 5th and 6th columns of Table 4). However, it is of interest to note that the results obtained with the three different approaches are largely consistent with each other and that there are only few samples where the results obtained with the use of the Holland & Powell (1998) v. Berman (1988) data sets differ.

The calculated pressures and the corresponding temperatures for the profile are shown in Fig. 7. For the further discussion we subdivided the data into three groups. Group I are medium-grade, mostly micaschist type rocks, from the northern 40 km of the transect. Group II are high-grade Plattengneiss type rocks from 40 to 60 km measured from the north end of the profile. Group III are medium grade rocks from the southern most 40 km of the transect. The data show that within Group I, the metamorphic grade increases from north to south. Pressure increases from 10 to

Table 4. Results of the model calculations (graphically illustrated in Fig. 7). The sample numbers (1st column) correspond to those shown on Fig. 2, the assemblage abbreviations (2nd column) to those of Table 2. The subscripts to the assemblage abbreviations correlate with different sets of reactions listed in Table 5. Column 3 are the P-T conditions of the water absent invariant points calculated with the phase diagram mode ('mode 1') of THERMOCALC. This is the data shown in Fig. 7. Column 4 are the calculated water activities ('mode 3' of THERMOCALC). The last two columns show the results of average P-T calculations (5th column; obtained with 'mode 2' of THERMOCALC) in comparison with results using WEBINVEQ (6th column). The three different modes of THERMOCALC choose their own sets of independent reactions, which cause slight incompatibilities between P-T results.

		H_2O ind. inv. point			AvPT		Webinveq	
Sample	Assemblage	T	P	$a(H_2O)$	T	P	T	P
1	MS_1	518 ± 57	10.2 ± 1.1	0.25	529 ± 25	10.8 ± 1.1	529 ± 27	10.4 ± 0.2
2	MS_{2a}	509 ± 45	9.2 ± 1.0	0.2884	559 ± 66	11.0 ± 3.8	544 ± 23	8.9 ± 0.6
3	MS_{2b}	575 ± 51	10.4 ± 1.2	0.4	597 ± 33	11 ± 1.6	633 ± 27	11.7 ± 0.7
6	PG_a	578 ± 50	10.5 ± 1.1	0.57	586 ± 21	10.4 ± 1.1	648 ± 25	10.9 ± 0.7
7	PG_a	536 ± 48	10.1 ± 1.1	0.2884	532 ± 24	9.7 ± 1.4	614 ± 24	10.6 ± 0.7
8	PG_a	642 ± 50	14 ± 1.2	0.5	638 ± 25	13.7 ± 1.4	735 ± 27	15.5 ± 0.8
9	PG_a	674 ± 57	10.4 ± 1.2	0.545	686 ± 26	10.8 ± 1.5	573 ± 27	8.3 ± 0.7
10	PG_a	594 ± 52	12.1 ± 1.2	0.5	598 ± 39	11.8 ± 2.0	636 ± 24	11.4 ± 0.7
11	PG_a	661 ± 32	12.9 ± 0.8	0.32	616 ± 21	12 ± 1.3	622 ± 26	12.2 ± 0.7
12	PG_b	711 ± 53	16.4 ± 1.4	0.23	705 ± 41	15.9 ± 1.9	768 ± 29	16.9 ± 0.8
13	PG_b	740 ± 53	14.2 ± 1.3	0.22	747 ± 39	14.3 ± 1.6	670 ± 29	12.1 ± 0.8
14	MS_{2c}	656 ± 51	10.1 ± 1.1	0.4	583 ± 24	10.4 ± 1.6	665 ± 24	11.1 ± 0.7
15	PG_b	690 ± 58	14.7 ± 1.4	0.32	685 ± 26	14.3 ± 1.4	685 ± 28	13.4 ± 0.8
16	PG_c	669 ± 61	14.9 ± 1.5	0.26	634 ± 28	13.9 ± 1.8	728 ± 29	16.8 ± 0.8
17	PG_b	739 ± 57	15 ± 1.4	0.26	736 ± 40	14.6 ± 1.6	790 ± 30	16.1 ± 0.8
18	PG_b	716 ± 59	14.5 ± 1.4	0.34	714 ± 34	14.1 ± 1.7	752 ± 30	13.6 ± 0.8
19	PG_b	690 ± 68	15.8 ± 1.5	0.21	581 ± 57	15.2 ± 2.5	696 ± 30	14.4 ± 0.8
20	PG_c	610 ± 5	13.4 ± 1.3	0.135	609 ± 26	13.2 ± 1.1	615 ± 26	11.5 ± 0.7
21	PG_c	613 ± 48	12.2 ± 1.1	0.155	612 ± 26	12.2 ± 1.2	613 ± 26	10.8 ± 0.7
22	PG_d	674 ± 22	10.3 ± 0.9	0.89	659 ± 32	10.3 ± 1.7	566 ± 24	8.2 ± 0.6
23	PG_b	685 ± 57	15.7 ± 1.4	0.0955	677 ± 86	15 ± 3.2	706 ± 28	14.1 ± 0.8
24	PG_e	600 ± 51	10.6 ± 1.1	0.27	603 ± 20	10.9 ± 1.2	598 ± 26	9.6 ± 0.7
25	PG_a	598 ± 58	9.3 ± 1.2	0.35	595 ± 21	8.9 ± 1.2	912 ± 32	14.9 ± 0.8
26	PG_e	660 ± 63	11.9 ± 1.3	0.91	658 ± 22	11.9 ± 1.2	719 ± 27	12.7 ± 0.7
28	PG_e	627 ± 67	11.2 ± 1.4	0.47	617 ± 40	10.3 ± 2.3	650 ± 30	10.7 ± 0.7

Table 5. End member reactions used for the thermobarometric calculations with THERMOCALC. Reactions with superscript[1] are those used for the calculation of the water invariant points and reactions (mode 1 of THERMOCALC). Reactions with * are those used for the average *PT* calculations (mode 2 of THERMOCALC). Note that all reactions are mineral end member reactions using the end member definitions used by THERMOCALC. For example, muscovite refers to the $KAl_3Si_3O_{12}H_2$ end member of white mica, but not to any white mica phase observed in thin section.

Assemblage MS_1:	Assemblage PG:
An + Phl = Ms + Prp + Grs[1]	Phl + Ky + Qtz = Prp + Ms[1]
An + Ann = Ms + Grs + Alm[1]	Phl + An = Prp + Grs + Ms[1]
Prp + Ann = Alm + Phl[1]	Grs + Ky + Qtz = An[1]
Ms + Phl + Qtz = Cel + Prp*	**PG_a**:
An + Phl = Ms + Prp + Grs*	Grs + Ky + Qtz = An*
An + Ann = Ms + Grs + Alm*	Pg + An = Grs + Ab + H_2O + Ky*
Pg + Prp + Ann + Qtz = Cel + Alm + Ab + H_2O*	Phl + Qtz + Ky = Prp + Ms*
	Ann + An = Grs + Alm + Ms*
Assemblage MS_2:	**PG_b**:
Phl + Ky + Qtz = Prp + Ms[1]	Grs + Qtz + Ky = An*
Phl + An = Prp + Grs + Ms[1]	Ann + Qtz + Ky = Alm + Ms*
Grs + Ky + Qtz = An[1]	Phl + An = Prp + Grs + Ms*
	Prp + Ms + Pg = Phl + Ab + H_2O + Ky*
MS_{2a}:	**PG_c**:
Grs + Ky + Qtz = An*	Grs + Qtz + Ky = An*
Pg + An = Grs + Ky = Prp + Ms*	Phl + Qtz + Ky = Prp + Ms*
Ann + Qtz + Ky = Alm + Ms*	Ann + Qtz + Ky = Alm + Ms*
Mrg + Phl + Ab = Prp + Grs + Ms + Pg*	Prp + Ms + Pg = Ab + Phl + H_2O + Ky*
MS_{2b}:	**PG_d**:
Grs + Qtz + Ky = An*	Grs + Qtz + Ky = An*
Mrg + Qtz = Grs + H_2O + Ky*	An + Pg = Grs + Ab + H_2O + Ky*
Grs + Pg + Qtz + Ky = Mrg + Ab*	Phl + Qtz + Ky = Prp + Ms*
Phl + Qtz + Ky = Prp + Ms*	Ann + Qtz + Ky = Alm + Ms*
Ann + Qtz + Ky = Alm + Ms*	
MS_{2c}:	**PG_e**:
Grs + Qtz + Ky = An*	Grs + Qtz + Ky = An*
Mrg + An = Grs + H_2O + Ky*	Pg + An = Grs + Ab + H_2O + Ky*
Grs + Pg + Qtz + Ky = Mrg + Ab*	Phl + Qtz + Ky = Prp + Ms*
Phl + Qtz + Ky = Prp + Ms*	Ann + Qtz + Ky = Alm + Ms*
Ann + Qtz + Ky = Alm + Ms*	

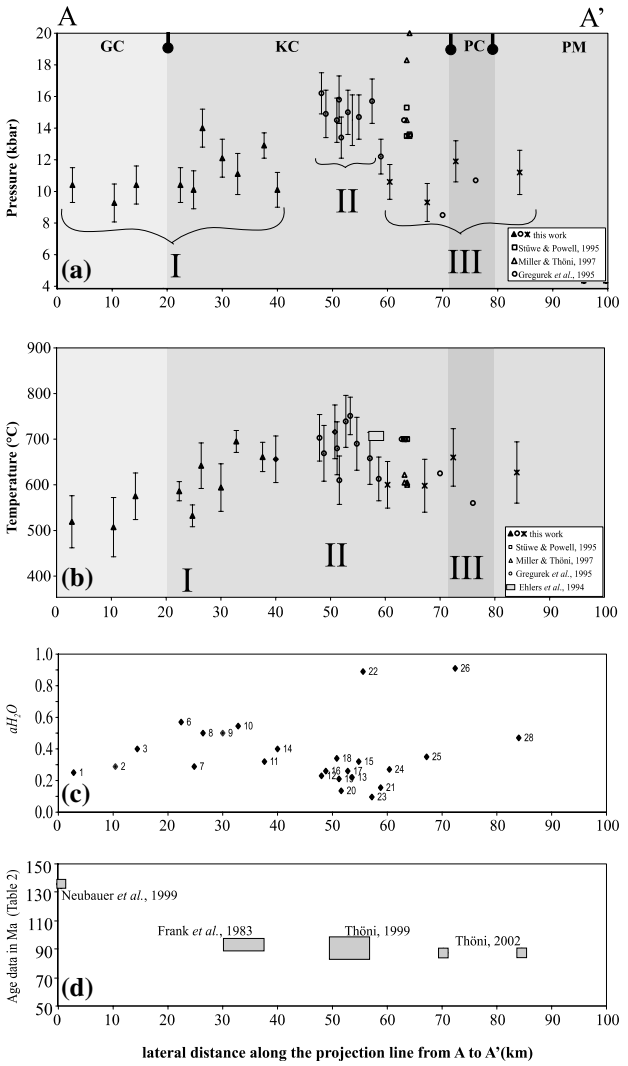

Fig. 7. Metamorphic field gradients of the Koralpe transect. (a) shows the changes of pressure with distance along the transect shown in Fig. 2. (b) shows the changes in temperature along this transect. (c) shows the corresponding changes in water activity. (d) shows some age data from the literature from Table 1. The width of the shaded boxes indicates the north–south coverage of the date, the height the errors quoted in the literature. All shown *P-T* results are those obtained using THERMOCALC (those from Table 4, column 3).

14 kbar (with a maximum standard deviation of ± 1.5 kbar) and temperature increases from 500 to 700 °C (with a maximum standard deviation per sample of ± 68 °C). The trend of this increase is gradual with respect to temperature but slightly discontinuous with respect to pressure. Within Group I, the field gradient is 5 °C km^{-1}, and 0.1 kbar km^{-1}. Within Group II (Plattengneiss) pressure is around 15 kbar and temperature around 700 °C. Both pressure and temperature show a sharp drop from Group II to Group III from 15 kbar to 10 kbar ± 1.5 kbar and from 700 °C to 600 °C ± 68 °C within a distance of 10 km. Within Group III, pressures remain around 10 kbar and temperatures around 600 °C.

The calculated water activities across the transect correlate to some extent with the *P–T* estimates, so that highest grade rocks are characterized by the lowest water activity (Fig. 7c). Within Group I a_{H_2O} varies between 0.25 and 0.57, and it appears that there is first an increase and later a decrease in a_{H_2O} from north to south. Within Group II a_{H_2O} is generally low and < 0.34. Within Group III, the a_{H_2O} rises again from north to south from 0.27 to 0.47. Samples 22 and 26 (from Group II and Group III, respectively) have higher values indicating that they had higher water contents during the metamorphic peak. This is also shown by the fact that they contain some retrograde minerals which were, however, not used as part of the *P–T* calculations.

DISCUSSION

Throughout this paper we assume that the *P–T* estimates represent the Eo-Alpine metamorphic peak. Thus, the data presented in Fig. 7 are interpreted as

the metamorphic conditions developed during subduction of the oceanic domain (Thöni & Jagoutz, 1993), and associated eclogitization of the rocks at a time where the nappe pile was thickest. In order to interpret the subsequent exhumation process, we will discuss in the following section some interpretations of the spatial changes of metamorphic grade (from our results above) and time of peak metamorphism (from the literature).

Grade and timing relationships

In the following section we interpret the northern part of the transect (the northern 60 km, Group I and II samples) in terms of two relationships that provide invaluable information on the nature of the orogenic process (Richardson & England, 1979): (1) the *P–T* slope of the data, and (2) the relationship between metamorphic grade and time of peak metamorphism. The *P–T* slope of the data is illustrated in Fig. 8(a), which shows that the collective data from the field gradient have a somewhat steeper slope than most meaningful metamorphic geotherms. The relationship between metamorphic grade and time of peak metamorphism can be inferred by a comparison of Fig. 7(b) and 7(d). This shows that peak metamorphism in the high grade parts of the transect occurred later (90 Ma, Thöni & Jagoutz, 1993) than in the low grade parts (130 Ma, Neubauer *et al*., 1999).

Interestingly, the slope of the data shown in Fig. 8(a) and the metamorphic grade-timing relationships (Fig. 7c,d) give rise to contrasting interpretations in terms of very simple orogenic models as pioneered by Richardson & England (1979). These authors showed that metamorphic field gradients should be interpreted in terms of a piezothermal array, if there was no syn- or postmetamorphic deformation that caused telescoping or disruption of the isograds. They defined a piezothermal array as the line that connects the metamorphic temperature peaks through depth and time for a transect of rocks exposed at the surface. Piezothermal arrays are characterized by two features, which both may be observed in the field: (1) their slope in *P/T* space, and (2) the relationship between timing of peak metamorphism and metamorphic grade. During regional metamorphism the *P/T* slope of piezotherms is likely to be steeper than any one metamorphic geotherm (Richardson & England, 1979). For regional metamorphic terranes, Richardson & England (1979) showed that this relationship between timing of peak metamorphism and metamorphic grade is likely to be characterized by later metamorphism with higher grade (Fig. 8d, (i)). This relationship has shown to hold for a number of terranes and a range of much more sophisticated models including some for the western Alps (Bousquet *et al*., 1997; Jamieson *et al*., 2002).

For the northern part of the transect investigated here, the *P–T* slope of the field gradient is inconsistent with classic models for regional metamorphism where erosion is the principal exhuming mechanism. In contrast, the timing relationships along the gradient (point 2 from above) are consistent with regional metamorphic models. Keeping this in mind, we will now interpret the metamorphic field gradient in terms of a tectonic model.

Exhumation of the Koralpe transect

In order to provide a basis for the following tectonic discussion, Fig. 9(a) shows a scaled reproduction of Fig. 7(a) and (b) in which pressure is converted to depth with 1 km $\approx$ 0.29 kbar (using a density of rocks of 2900 kg m^{-3}) and in which there is no vertical

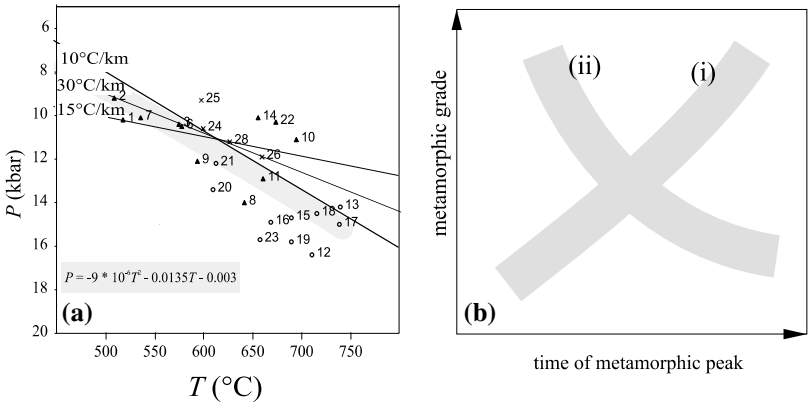

Fig. 8. Correlation between different data sets from the field gradient shown in Fig. 7. (a) *P-T* diagram showing the collective data from Fig. 7. Sample numbers refer to those shown on Fig. 2. (b) Cartoon showing relationship between peak metamorphic temperature and time of peak metamorphism for different heating models. A positive correlation is typical for regional metamorphic terranes (Richardson & England, 1979), which is shown as the curve 'i'. A negative correlation (shown as curve 'ii') is typical for advectively heated (Greenfield *et al*., 1998). The difference between these relationships was discussed by several authors (Harrison & Clarke, 1979; Stüwe & Powell, 1997; Stüwe, 1998) but is rarely used as an explanatory tool for field gradients.

exaggeration. On the same profile, temperature converted to depth is shown using a gradient of 13 °C km^{-1}, which is based on the assumption that the peak P/T ratio of the Plattengneiss (15 kbar/700 °C) shows a representative geothermal gradient at Eo-Alpine times. Before embarking on the tectonic interpretation of this figure, three points are noted:

(1) The eclogites of the type locality record pressures that are only a little higher than those of the surrounding pelites. This may be because they record an earlier stage of the P–T path, or because they were at greater depths prior to the M2/D2 event discussed here. However, during and after the deformation and metamorphic events discussed in this paper, the eclogites can be considered to be part of the overall Koralpe sequence. We therefore rely on the peak conditions derived from the assemblages in the D2 fabric in the surrounding pelites.

(2) All rocks along the transect were exhumed a total of 30 km (z_a in Fig. 9a). In addition there is some 30–40 km of differential exhumation (Δz in Fig. 9a) between different rocks on various parts of the profile. Here we discuss only tectonic processes that may account for the differential exhumation. The uniform exhumation of z_a is assumed to have occurred by erosion (in the absence of any other evidence).

(3) In view of the inconsistencies of the grade-timing relationships discussed in the last section, we note that a number of physical processes have been discussed in the literature that may have had an influence on the thermal and baric evolution of the Koralpe which may hinder a simple tectonic interpretation in terms of a cross sectional model explaining the exhumation geometry. For example, because of the unusual high P/T gradient of the data shown in Fig. 8(c), shear heating and advective heat sources have been discussed as potentially contributing to the thermal evolution (Stüwe, 1998; Stüwe & Powell, 1997), and tectonic overpressure may have had some influence on the pressures recorded by the parageneses (Tenczer *et al.*, 2001). Stüwe (1998) has also stressed the fact that metamorphism and deformation occurred synchronously in the Koralpe transect which is inconsistent with an interpretation using classic regional metamorphic models. Finally, measurements of thermal conductivities and radioactivities are currently being undertaken, and it is possible that lateral variations of these parameters play an important role for the interpretation of the P–T conditions (Mauritsch, pers. comm. 2002).

Keeping these points in mind, we suggest that the grade–timing relationships discussed above must not be interpreted in terms of thermal processes alone, but that these must also be interpreted in terms of tectonic processes. As derived from Fig. 9(a), this exhumation gradient is of the order of 1 km vertical per 2.5 km lateral. Interestingly, this continuous gradient crosses the boundary between the Gleinalm and the Koralpe complexes, which has traditionally been interpreted to

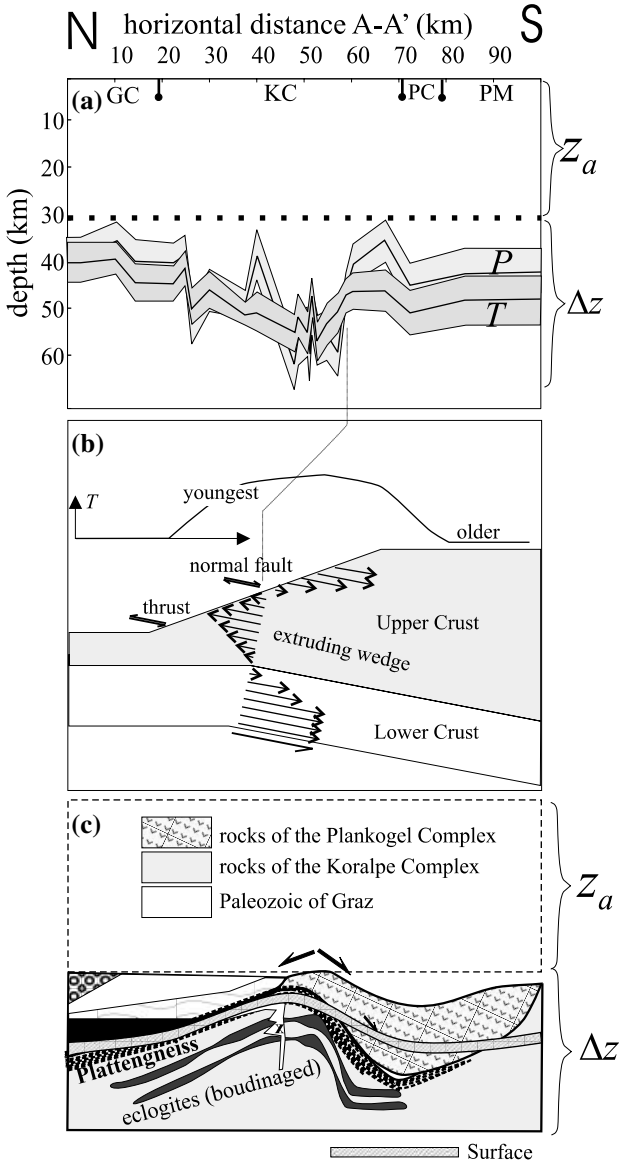

Fig. 9. Comparison between data and potential tectonic models. (a) shows a scaled reproduction of Fig. 7(a, b). Both P and T (here as black lines; the standard deviation is outlined by grey-shaded fields) are translated into depth assuming a pressure gradient of 0.29 kbar km^{-1} depth and a temperature gradient of 13 °C km^{-1} in depth. z_a is the amount of overall exhumation which is treated to be homogeneous along the transect in absence of any better information. Δz is differential exhumation which is represented by the changing values in P and T along the transect and is interpreted in terms of tectonic models. (b) shows a tectonic model by Jamieson *et al.* (2002) showing the interaction between ductile extrusion of a continental wedge during compression and erosion. The geometry of the model may describe the features of the transect quite well. It discusses also the distribution of the metamorphic grade along a profile (T is in this case the metamorphic peak temperature) and time of T, given here only as relative ages (younger and older). (c) shows a tectonic reconstruction of the whole transect and is modified after Kurz *et al.* (2002). Signatures of different rock types which are not given in this figure correspond to those of Fig. 2.

be a major tectonic boundary (Becker, 1980; Frank *et al.*, 1983; Frank, 1987). Our results indicate that this boundary, if it exists at all, must be older than the Eo-Alpine metamorphic event. In contrast, a more abrupt decrease in metamorphic grade from north to south occurs some 60 km from the northern end of the transect. It is suggested that this decrease is related to the normal faulting between the Plankogel and the Koralpe complexes that has been described by Kurz *et al.* (2002). The Plankogel Complex has long been interpreted as tectonically juxtaposed against the Koralpe Complex (Frank *et al.*, 1983; Gregurek *et al.*, 1997).

These observations are consistent with a recently published model of Jamieson *et al.* (2002) who provided models of various cases for the interaction of metamorphism, deformation and exhumation in large convergent orogens (Fig. 9b). The best model to explain the exhumation of the Koralpe rocks after subduction is one involving focused erosion affecting exhumation of a mid-crustal channel flow. It allows deep seated rocks to be exhumed by an extruding wedge leading to a thrust and normal fault geometry as observed here. The peak grade profile of the model makes a good fit to our observations, and also the grade–timing relationship is supported by the trend of the geochronological data known in the Koralpe. The model of Jamieson *et al.* (2002) as well as our data summarized in Fig. 9(a) are both largely consistent with the tectonic reconstruction of Kurz *et al.* (2002) shown in Fig. 9(c).

The Koralpe transect in a regional context

In all previous sections the data are interpreted in terms on a *two* dimensional N–S cross-section through the Koralpe. However, there are aspects of the *three* dimensional geometry of the Koralpe region that may also have played a role in the final geometry of the transect and which have not been discussed above. These are:

(1) The Koralpe region was folded after the M2/D2 event into antiforms and synforms at the km scale (Fig. 2b). In the northern part of the study area, the Gleinalpe Complex forms a large antiform (Neubauer *et al.*, 1995), but the amplitude of these folds is not large enough to influence the interpretation of the barometry along the transect. (2) The northern part of the transect is bounded by a system of sinistral strike slip zones and medium to high angle ductile normal faults forming a NE–SW striking wrench corridor (Neubauer *et al.*, 1995). This wrench corridor plays an important role in the exhumation and the final geometry of the Koralpe region. It was also associated with the formation of the Cretaceous Gosau basin (Kainach Gosau) immediately east of the Koralpe. Interestingly, this basin formed simultaneously with the onset of rapid exhumation of the Koralpe (Neubauer *et al.*, 1995), but contains no sedimentary components of the crystalline Koralpe. (3) Fission track studies of Hejl (1997) show that the northern Koralpe and the surrounding Austroalpine crystalline basement cooled below 200 °C at 50 Ma and have never been heated again. Further south, fission track ages are younger (30 Ma) indicating differential exhumation from north to south (Hejl, 1997).

CONCLUSIONS

(1) The metamorphic field gradient of Eo-Alpine parageneses (90 Ma) in the eclogite type locality in the Koralpe, Eastern Alps, Austria can be divided into three parts: (I) a northern part where metamorphic peak P–T increase from north to south (II) a high grade central part and (III) a southern part where the conditions decrease again. In the first part (Group I samples) of the transect metamorphic temperatures increase from 500 to 700 °C and pressures increase from 10 to 14 kbar over a section of 40 km from north to south (corresponding to metamorphic field gradients of 5 °C km^{-1} and 0.1 kbar km^{-1}, respectively). In part II (Group II samples) peak metamorphic conditions are around 15 kbar and 700 °C over about 20 km of the transect. In part III (Group III samples) peak conditions decrease from 15 to 10 kbar and 700–600 °C within 10 km and then remain largely constant over the remaining 30 km of the profile.

(2) We suggest that the largely continuous increase of P–T along the northern part of the transect indicates that there were no discrete major tectonic boundaries separating the various crustal blocks during or after the Eo-Alpine event. However, the penetrative deformation of the whole pile along the Plattengneiss shear zone is responsible for the baric variation along the transect.

(3) In the south, the contact between the Plankogel complex and Koralpe is assumed to be an Eo-Alpine normal fault zone leading to syn-orogenic extension and oblique differential exhumation of the deep-seated rocks.

(4) The overall T/P ratio of the data is generally low. This indicates that the transect was largely isothermal at Eo-Alpine times over a large depth range. This indicates that the field gradient is unlikely to represent a geotherm and is more likely to be interpreted in terms of a piezothermal array. It also may imply that heat production and/or heat advection processes may have played a role for the formation of the metamorphic field gradient.

(5) The piezothermal array of the Koralpe transect has two incompatible characteristics: (i) It is characterized by an increasing age with decreasing metamorphic grade. This is consistent with the timing relationships along piezothermal arrays predicted by simple models for regional metamorphism. (ii) It is characterized by a T/P gradient that is lower than for common metamorphic geotherms. This feature is inconsistent with piezothermal arrays predicted by models for regional metamorphism. A simple model for regional

metamorphism in terms of a piezothermal array is therefore insufficient for the interpretation of the formation of the whole field gradient and might only be applied to the northern part of the study area.
(6) The spatial distribution of P–T in the whole transect may be best explained by a tectonic model assuming large-scale convergence and exhumation by syn-convergent erosion.

This scenario leads to the extrusion of a ductile wedge in the central part of the orogen, forming comparable tectonic features to the study area and explaining well the temporal and thermal relationship of the rocks during peak metamorphism.

ACKNOWLEDGEMENTS

This study has been supported FWF (Austrian Science Foundation) P12846-GEO. We acknowledge the support of the European Community Access to Research, Infrastructure action of the Improving Human Potential Programme, contract HPRI-CT-1999–00008 awarded to Prof. B. J. Wood (EU Geochemical Facility, University of Bristol). The Department of Mineralogy and Petrology in Leoben and Graz supported us with the use of the analytical facilities. For their continued help and interesting discussions we thank K. Ettinger, R. Kaindl, A. Proyer, H. Mühlhans, G. Habler, W. Kurz, H. Fritz and C. Biermeier. P. Tropper R. Bousquet and an anonymous reviewer are thanked for a large range of constructive criticisms which helped substantially to improve this manuscript. T. Barr is thanked for his invaluable efforts in improving the English in the final version of this manuscript.

REFERENCES

Becker, L. P., 1980. Erläuterungen zu Blatt 162, Köflach. *Geologische Bundesanstalt*, pp. 57.

Berman, R. G., 1988. Internally-consistent thermodynamic data for stoichiometric minerals in the system Na_2O-K_2O-CaO-MgO-FeO-Fe_2O_3-Al_2O_3-SiO_2-TiO_2-H_2O-CO_2. *Journal of Petrology*, **29,** 445–522.

Bousquet, R., Goffe, B., Henry, P., LePichon, X. & Chopin, C., 1997. Kinematic, thermal and petrological model of the Central Alps: Lepontine metamorphism in the upper crust and eclogitisation of the lower crust. *Tectonophysics*, **273,** 105–127.

Dallmeyer, R. D., Neubauer, F., Handler, R., Fritz, H., Mueller, W., Pana, D. & Putis, M., 1996. Tectonothermal evolution of the internal Alps and Carpathians; evidence from $^{40}Ar/^{39}Ar$ mineral and whole-rock data. *Eclogae Geologicae Helvetiae*, **89,** 203–227.

Droop, G. T. R., Lombardo, B. & Pognante, U., 1990. Formation and distribution of eclogite facies rocks in the Alps. In: *Eclogite Facies Rocks* (ed. Carswell, D. A.), pp. 225–259. Blackie, Glasgow.

Ehlers, K., Stüwe, K., Powell, R., Sandiford, M. & Frank, W., 1994. Thermometrically inferred cooling rates from the Plattengneis, Koralm region, Eastern Alps. *Earth and Planetary Science Letters*, **125,** 307–321.

Flügel, H. W. & Neubauer, F., 1984. *Erläuterungen zur geologischen Karte der Steiermark 1: 200000*. Geologische Bundesanstalt, Vienna.

Frank, W., 1987. Evolution of the Austroalpine elements in the Cretaceous. In: *Geodynamics of the Eastern Alps* (eds Flügel, H. W. & Faupl, P.), pp. 379–406. Deuticke, Vienna.

Frank, W., Esterlus, M., Frey, I., Jung, G., Krohe, A. & Weber, J., 1983. Die Entwicklungsgeschichte von Stub- und Koralpenkristallin und die Beziehung zum Grazer Paläozoikum. *Hochschulschwerpunkt*, **15,** 263–293.

Frey, M., Desmons, J. & Neubauer, F., 1999. The new metamorphic map of the Alps: Introduction. *Schweizer Mineralogische und Petrographische Mitteilungen*, **79,** 1–4.

Gordon, T. M., 1998. WEBINVEQ thermobarometry; an experiment in providing interactive scientific software on the World Wide Web. *Computers and Geosciences*, **24,** 43–49.

Greenfield, J. E., Clarke, G. L. & White, R. W., 1998. A sequence of partial melting reactions at Mt Stafford, central Australia. *Journal of Metamorphic Geology*, **16,** 363–378.

Gregurek, D., Abart, R. & Hoinkes, G., 1997. Contrasting eoalpine P-T evolutions in the southern Koralpe, Eastern Alps. *Mineralogy and Petrology*, **60,** 61–80.

Habler, G. & Thöni, M., 2001. Preservation of Permo-Triassic low-pressure assemblages in the Cretaceous high-pressure metamorphic Saualpe crystalline basement (Eastern Alps, Austria). *Journal of Metamorphic Geology*, **19,** 679–697.

Harrison, T. M. & Clarke, G. K., 1979. A model of the thermal effects of igneous intrusion and uplift as applied to Quottoon pluton, British Columbia. *Canadian Journal of Earth Science*, **16,** 410–420.

Hauy, R. J., 1822. *Traité de Mineralogie*, 2nd edn. Bachelier, Paris.

Heede, H. U., 1997. Isotopengeologische Untersuchungen an Gesteinen des ostalpinen Saualpenkristallins, Kärnten-Österreich. *Münstersche Forschungen Zur Geologie und Paläontologie*, **81,** 1–168.

Hejl, E., 1997. 'Cold spots' during the Cenozoic evolution of the Eastern Alps: thermochronological interpretation of apatite fission-track data. *Tectonophysics*, **272,** 159–173.

Hinterlechner-Ravnik, A., Sassi, F. P. & Visona, D., 1991. The Austridic eclogites, metabasites and metaultrabasites from the Pohorje area (Eastern Alps, Yugoslavia). I. The eclogites and related rocks. *Atti della Accademia Nazionale dei Lincei. Rendiconti Lincei. Scienze Fisiche E Naturali*, **2,** 157–173.

Hoinkes, G., Frank, W., Mauracher, J., Peschel, R., Purtscheller, F. & Tessadri, R., 1987. Petrography of the Schneeberg Complex. In: *Geodynamics of the Eastern Alps* (eds Flügel, H. W. & Faupl, P.), pp. 190–199. Deuticke, Vienna.

Hoinkes, G., Kostner, A. & Thöni, M., 1991. Petrologic constraints for eoalpine eclogite facies metamorphism in the Austroalpine Ötztal basement. *Mineralogy and Petrology*, **43,** 237–254.

Holland, J. T. B. & Powell, R., 1998. An internally consistent thermodynamic data set for phases of petrological interest. *Journal of Metamorphic Geology*, **16,** 309–343.

Inger, S. & Cliff, R. A., 1994. Timing of metamorphism in the Tauern Window, Eastern Alps: Rb-Sr ages and fabric formation. *Journal of Metamorphic Geology*, **12,** 695–707.

Jamieson, R. A., Beaumont, C., Nguyen, M. H. & Lee, B., 2002. Interaction of metamorphism, deformation and exhumation in large convergent orogens. *Journal of Metamorphic Geology*, **20,** 9–24.

Jung, G., 1982, Geologische und Geochronologische Untersuchungen Des Metamorphoseablaufes in Glein-, Stub- und Koralpe. *PhD Thesis*, *University of Vienna, Vienna*.

Konzett, J. & Hoinkes, G., 1991. High pressure metamorphism in the Austroalpine Schneeberg Complex and adjacent Oetztal basement rocks. *Terra Abstracts*, **3,** 88–89.

Konzett, J. & Hoinkes, G., 1996. Paragonite-hornblende assemblages and their petrological significance; an example from the Austroalpine Schneeberg Complex, southern Tyrol, Italy. *Journal of Metamorphic Geology*, **14,** 85–101.

Kretz, R., 1983. Symbols for rockforming minerals. *American Mineralogist*, **68,** 277–279.

Krohe, A., 1987. Kinematics of Creatceaous nappe tectonics in the Austroalpine basement of the Koralpe region (eastern Austria). *Tectonophysics*, **136,** 171–196.

Kurz, W., Fritz, H., Tenczer, V. & Unzog, W., 2002. Tectonometamorphic evolution of the Koralm Complex (Eastern Alps): Constraints from microstructures and textures of the 'Plattengneis' – shear zone. *Journal of Structural Geology*, **24,** 1957–1970.

Kurz, W., Neubauer, F. & Dachs, E., 1998. Eclogite meso- and microfabrics; implications for the burial and exhumation history of eclogites in the Tauern Window (Eastern Alps) from *P-T-d* paths. *Tectonophysics*, **285,** 183–209.

Kurz, W., Neubauer, F. & Genser, J., 1996. Kinematics of Penninic nappes (Glockner Nappe and basement-cover nappes) in the Tauern Window (Eastern Alps, Austria) during subduction and Penninic-Austroalpine collision. *Eclogae Geologicae Helvetiae*, **89,** 573–605.

Lammerer, B. & Weger, M., 1998. Footwall uplift in an orogenic wedge; the Tauern Window in the Eastern Alps of Europe. *Tectonophysics*, **285,** 213–230.

Lichem, Ch, Hoinkes, G. & Gregurek, D., 1997. Polymetamorphism of the Austroalpine Koralm basement: New evidence for a Permian event. *Terra Nova*, **9,** 489.

Miller, Ch & Thöni, M., 1997. Eo-Alpine eclogitisation of Permian MORB-type gabbros in the Koralpe (Eastern Alps, Austria): new geochronological, geochemical and petrological data. *Chemical Geology*, **137,** 283–310.

Morauf, W., 1980. Die permische Differentiation und die alpidische Metamorphose des Granitgneises von Wolfsberg, Koralpe, SE-Ostalpen, mit Rb-Sr- und K-Ar-Isotopenbestimmungen. *Tschermaks Mineralogische und Petrographische Mitteilungen*, **27,** 169–185.

Morauf, W., 1981. Rb-Sr- und K-Ar-Isotopen-Alter an Pegmatiten aus Kor- und Saualpe, SE-Ostalpen, Oesterreich. *Tschermaks Mineralogische und Petrographische Mitteilungen*, **28,** 113–129.

Neubauer, F., 1987. Bau und Entwicklungsgeschichte des Rennfeld-Mugel- und des Gleinalm-Kristallins (Ostalpen). *Abhandlungen der Geologischen Bundesanstalt (Geologie, Geochemie, Tektonik)*, **42,** 137.

Neubauer, F., Dallmeyer, R. D., Dunkl, I. & Schirnik, D., 1995. Late Cretaceous exhumation of the metamorphic Gleinalm dome, Eastern Alps: kinematics, cooling history and sedimentary response in a sinistral wrench corridor. *Tecnophysics*, **242,** 79–98.

Neubauer, F. & Genser, J., 1990. Architektur und Kinematik der östlichen Zentralalpen – eine Übersicht. *Mitteilungen Des Naturwissenschaftlichen Vereins der Steiermark*, **120,** 203–219.

Neubauer, F., Hoinkes, G., Sassi, F. P., Handler, R., Hoeck, V., Koller, F. & Frank, W., 1999. Pre-Alpine metamorphism of the Eastern Alps. *Schweizerische Mineralogische und Petrographische Mitteilungen*., **79,** 41–62.

Paquette, J. L. & Gebauer, D., 1991. U-Pb zircon and Sm-Nd isotopic study on eclogitized meta-basic and metal-acidic rocks of the Koralpe, Eastern Alps, Austria. *Terra Abstracts*, **3,** 505.

Powell, R. & Holland, T. J. B., 1988. An internally consistent thermodynamic dataset with uncertainties and correlations: 3. Application methods, worked examples and a computer program. *Journal of Metamorphic Geology*, **6,** 173–204.

Richardson, S. W. & England, P. C., 1979. Metamorphic consequences of crustal eclogite production in overthrust orogenic zones. *Earth and Planetary Science Letters*, **42,** 183–190.

Schuster, R., Bernhard, F., Hoinkes, G., Kaindl, R., Koller, F., Leber, T., Melcher, F. & Puhl, J., 1999. Excursion to the Eastern Alps; metamorphism at the eastern end of the Alps-Alpine, Permo-Triassic, Variscan? *Berichte der Deutschen Mineralogischen Gesellschaft*, **2,** 111–136.

Schuster, R. & Thöni, M., 1996. Permian Garnet: Indications for a regional Permian metamorphism in the southern part of the Austroalpine basement units. *Mitteilungen der Österreichischen Mineralogischen Gesellschaft*, **141,** 219–221.

Stüwe, K., 1998. Heat sources of Cretaceous metamorphism in the Eastern Alps – a discussion. *Tectonophysics*, **287,** 251–269.

Stüwe, K. & Ehlers, K., 1996. The qualitative zoning record of minerals. A method for determining the duration of metamorphic events? *Mineralogy and Petrology*, **56,** 171–184.

Stüwe, K. & Powell, R., 1995. *PT* paths from modal proportions: application to the Koralm Complex, Eastern Alps. *Contributions to Mineralogy and Petrology*, **119,** 83–93.

Stüwe, K. & Powell, R., 1997. Reaction Enthalpies of Subsolidus Equilibria in Pelitic Rocks. Magnitude and Influence on Cretaceous Metamorphism of the Koralm Complex, Eastern Alps. *Mitteilungen Des Naturwissenschaftlichen Verein für Steiermark*, **127,** 45–60.

Tenczer, V., Stüwe, K. & Barr, T. D., 2001. Pressure anomalies around cylindrical objecs in simple shear. *Journal of Structural Geology*, **23,** 777–788.

Thöni, M., 1994. Variscan vs. Alpine eclogites in the Eastern Alps; geochronology and isotope geochemistry. *Mitteilungen der Oesterreichischen Mineralogischen Gesellschaft*, **139,** 118.

Thöni, M., 1999. A review of geochronological data from the Eastern Alps. *Schweizerische Mineralogische und Petrographische Mitteilungen*, **79,** 209–230.

Thöni, M., 2002. Sm-Nd isotope systematics in garnet from different lithologies (Eastern Alps) – age results, and an evaluation of potential problems for garnet Sm-Nd Chronometry. *Chemical Geology*, **194,** 353–379.

Thöni, M. & Jagoutz, E., 1992. Some new aspects of dating eclogites in orogenic belts: Sm-Nd, Rb-Sr, and Pb-Pb isotopic results from the Austroalpine Saualpe and Koralpe type-locality (Carinthia/Styria, southeastern Austria). *Geochimica et Cosmochimica Acta*, **56,** 347–368.

Thöni, M. & Jagoutz, E., 1993. Isotopic constraints for Eo-Alpine high-P metamorphism in the Austroalpine nappes of the Eastern Alps: bearing on Alpine orogenesis. *Schweizerische Mineralogische und Petrographische Mitteilungen*, **73,** 177–189.

Thöni, M. & Miller, Ch, 1996. Garnet Sm-Nd data from the Saualpe and the Koralpe (Eastern Alps, Austria): chronological and *P-T* constraints on the thermal and tectonic history. *Journal of Metamorphic Geology*, **14,** 453–466.

Thöni, M. & Miller, Ch, 2000. Permo-Triassic pegmatites in the Eo-Alpine eclogite-facies Koralpe Complex, Austria; age and magma source constraints from mineral chemical, Rb-Sr and Sm-Nd isotope data. *Schweizerische Mineralogische und Petrographische Mitteilungen*, **80,** 169–186.

Todd, C. S. & Engi, M., 1997. Metamorphic field gradients in the Central Alps. *Journal of Metamorphic Geology*, **15,** 513–530.

Weber, J., 1982, .Metamorphosestudien an Pelitischen Gesteinen der Wolfsberger Serie und der Tieferen Anteile Des Koralpenkristallins in Kärnten. *PhD Thesis*, *University of Vienna, Vienna*.

Wimmer-Frey, I., 1984. Gefüge- und Metamorphoseuntersuchungen am Plattengneis der zentralen Koralm, W-Steiermark. *PhD Thesis*, *University of Vienna, Vienna*.

Received 10 June 2001; revision accepted 10 February 2003.